Cell

Article

β-Neurexins Control Neural Circuits by Regulating Synaptic Endocannabinoid Signaling

Graphical Abstract

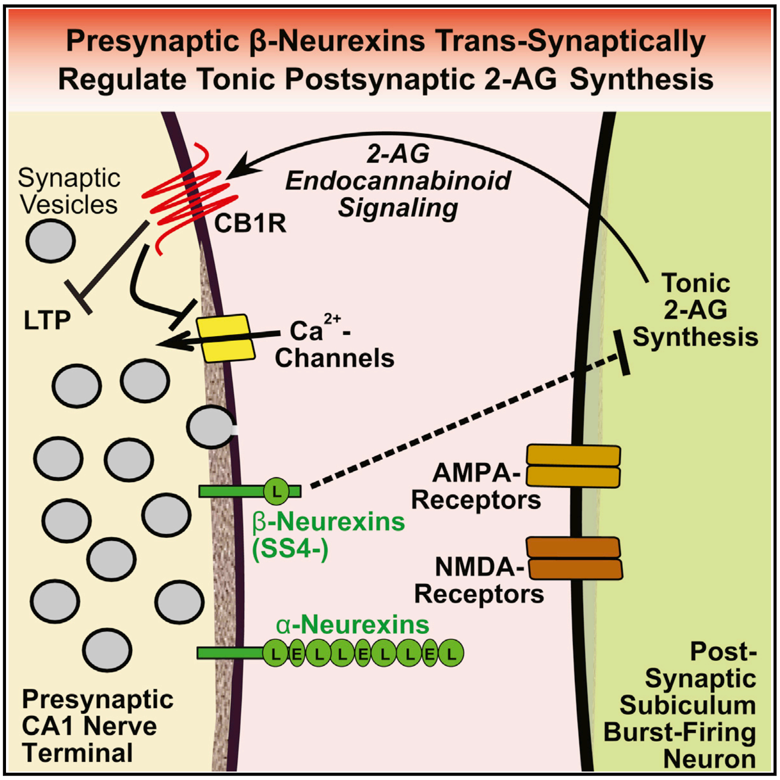

Highlights

- Conditional β-neurexin knockout decreases excitatory synapse release probability
- β-neurexins decrease tonic endocannabinoid signaling by suppressing 2-AG synthesis
- β-neurexins differentially regulate release at hippocampal subiculum synapses
- Conditional β-neurexins knockout in CA1-region neurons impairs contextual memory

Authors

Garret R. Anderson, Jason Aoto, Katsuhiko Tabuchi, ..., Lu Chen, Robert C. Malenka, Thomas C. Südhof

Correspondence

tcs1@stanford.edu

In Brief

β-neurexins have a surprisingly distinct and selective role in regulating neurotransmitter release in the hippocampus and in maintaining conceptual fear memories. They act to trans-synaptically downregulate tonic endocannabinoid signaling, whose presence at excitatory hippocampal neurons was unexpected.

Anderson et al., 2015, Cell *162*, 593–606
July 30, 2015 ©2015 Elsevier Inc.
http://dx.doi.org/10.1016/j.cell.2015.06.056

Cell

β-Neurexins Control Neural Circuits by Regulating Synaptic Endocannabinoid Signaling

Garret R. Anderson,[1,2] Jason Aoto,[1] Katsuhiko Tabuchi,[1,6] Csaba Földy,[1,2] Jason Covy,[1] Ada Xin Yee,[3] Dick Wu,[1,2] Sung-Jin Lee,[1] Lu Chen,[3] Robert C. Malenka,[2,4] and Thomas C. Südhof[1,5,*]
[1]Department of Molecular and Cellular Physiology
[2]Department of Psychiatry and Behavioral Sciences
[3]Department of Neurosurgery
[4]Nancy Pritzker Laboratory
[5]Howard Hughes Medical Institute
Stanford University Medical School, 265 Campus Drive, Stanford, CA 94305-5453, USA
[6]Department of Neurophysiology, Shinshu University School of Medicine, Matsumoto 390-8621, Japan
*Correspondence: tcs1@stanford.edu
http://dx.doi.org/10.1016/j.cell.2015.06.056

SUMMARY

α- and β-neurexins are presynaptic cell-adhesion molecules implicated in autism and schizophrenia. We find that, although β-neurexins are expressed at much lower levels than α-neurexins, conditional knockout of β-neurexins with continued expression of α-neurexins dramatically decreased neurotransmitter release at excitatory synapses in cultured cortical neurons. The β-neurexin knockout phenotype was attenuated by CB1-receptor inhibition, which blocks presynaptic endocannabinoid signaling, or by 2-arachidonoylglycerol synthesis inhibition, which impairs postsynaptic endocannabinoid release. In synapses formed by CA1-region pyramidal neurons onto burst-firing subiculum neurons, presynaptic in vivo knockout of β-neurexins aggravated endocannabinoid-mediated inhibition of synaptic transmission and blocked LTP; presynaptic CB1-receptor antagonists or postsynaptic 2-arachidonoylglycerol synthesis inhibition again reversed this block. Moreover, conditional knockout of β-neurexins in CA1-region neurons impaired contextual fear memories. Thus, our data suggest that presynaptic β-neurexins control synaptic strength in excitatory synapses by regulating postsynaptic 2-arachidonoylglycerol synthesis, revealing an unexpected role for β-neurexins in the endocannabinoid-dependent regulation of neural circuits.

INTRODUCTION

Synaptic cell-adhesion molecules play critical roles in establishing and restructuring synaptic connections throughout life. Neurexins are evolutionarily conserved presynaptic cell-adhesion molecules that engage in trans-synaptic interactions with multifarious postsynaptic ligands, including neuroligins (NLs), cerebellins, and LRRTMs (Krueger et al., 2012; Südhof, 2008). In mammals, neurexins are encoded by three genes, each of which contains independent promoters for longer α- and shorter β-neurexins (Rowen et al., 2002; Tabuchi and Südhof, 2002; Ullrich et al., 1995; Ushkaryov et al., 1992, 1994). β-neurexins are N-terminally truncated versions of α-neurexins that contain only a short (~40 residues) β-specific N-terminal sequence that then splices into the middle of the α-neurexin sequences (Ushkaryov et al., 1992). α- and shorter β-neurexin transcripts are extensively alternatively spliced at six canonical sites, resulting in over 1,000 distinct neurexin mRNAs (Ullrich et al., 1995; Treutlein et al., 2014).

Although neurexins are well studied, little is known about their fundamental functions. Ligands that bind to either both α- and β-neurexins (e.g., neuroligins, LRRTMs, dystroglycan, and cerebellins; Ichtchenko et al., 1995, Ko et al., 2009; de Wit et al., 2009; Siddiqui et al., 2010, Uemura et al., 2010) or only to α-neurexins (e.g., neurexophilins; Petrenko et al., 1996) have been described, and constitutive knockouts (KOs) of α-neurexins were shown to severely impair neurotransmitter release (Missler et al., 2003). However, only a limited understanding of α-neurexin functions is available, and little is known about β-neurexins. The lack of information on β-neurexin functions is particularly striking because nearly all biochemical studies on neurexins were performed with β-neurexins. Elucidating the synaptic actions of neurexins is a major technical challenge given their diversity and complexity. This challenge has taken on added importance given that hundreds of neurexin mutations were associated with several neuropsychiatric disorders (Südhof, 2008; Bang and Owczarek, 2013; Clarke and Eapen, 2014).

To specifically assess the function of β-neurexins, we generated mutant mice carrying conditional KO (cKO) alleles of all three β-neurexins. Despite a low abundance of β-neurexin transcripts, we found that KO of β-neurexins in cultured neurons in vitro and in hippocampus in vivo impaired neurotransmitter release at excitatory synapses. Surprisingly, this decrease was due, at least in part, to enhanced tonic activation of presynaptic CB1-receptors (CB1Rs), caused by increased postsynaptic synthesis of the endocannabinoid 2-arachidonoylglycerol (2-AG). Moreover, synapses of hippocampal CA1 pyramidal cells onto pyramidal neurons in the subiculum—the major output pathway of the hippocampus—were differentially regulated by endocannabinoids, and deletion of β-neurexins selectively

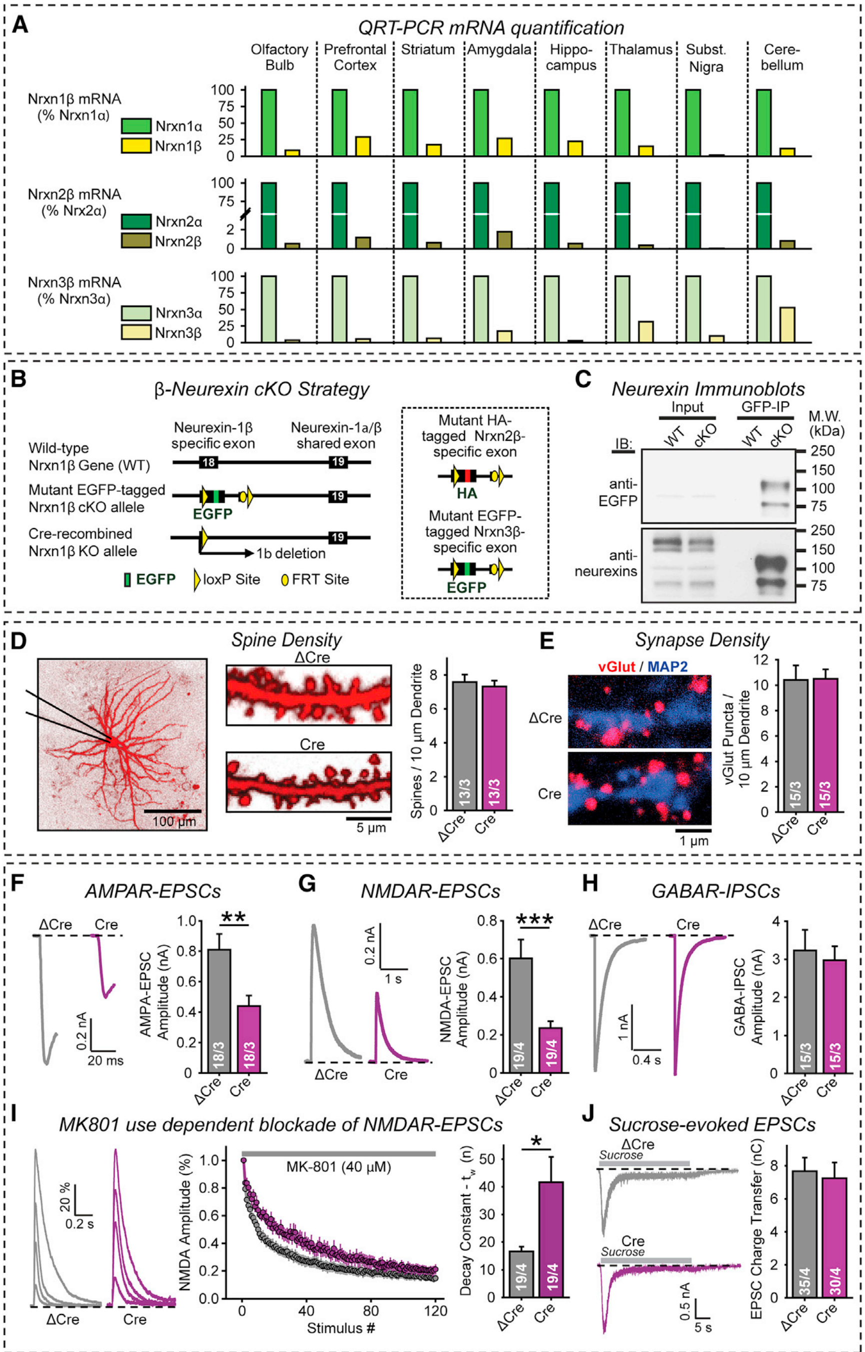

Figure 1. Conditional KO of β-Neurexins Impairs Excitatory Synaptic Transmission

(A) β-neurexins are expressed at levels 10- to 100-fold lower than those of α-neurexins. Data show relative α- and β-neurexin mRNA levels measured by qRT-PCR (n = 3 mice at P30).

(B) Conditional KO (cKO) strategy for neurexin-1β (left) and neurexin-2β and -3β (right, dashed box). All cKOs involve floxing the 5′ β-neurexin-specific exon and adding an N-terminal epitope tag (EGFP for neurexin-1β and -3β; HA-tag for neurexin-2β).

(C) Immunoblots of tagged β-neurexins in cKO mice with antibodies to GFP (top) and to a conserved C-terminal neurexin epitope (bottom). Proteins in cortex homogenates (from 3-week-old control and triple-β-neurexin cKO mice; input) were immunoprecipitated with GFP antibodies (GFP-IP) to visualize the low-abundance β-neurexins in cKO mouse samples.

(D) β-neurexin KO does not alter morphological parameters in cultured cortical neurons. (Left) Representative images of neurons filled with Alexa Fluor 594 via the patch pipette. (Right) Summary graphs of spine density.

(E) β-neurexin KO does not impair excitatory synapse density and size. (Left) Representative images; (right) summary graphs of vGlut1-positive synapse density.

(F–H) β-neurexin KO in cultured cortical neurons impairs excitatory, but not inhibitory, synaptic transmission evoked by isolated action potentials (F, AMPAR-mediated EPSCs; G, NMDAR-mediated EPSCs; H, GABAR-mediated IPSCs).

(I) β-neurexin KO decreases the presynaptic release probability, measured via the MK-801-induced progressive block of NMDAR-mediated synaptic responses. (Left) Representative EPSC traces for the 1st, 10th, 25th, and 125th stimulus. (Center) Mean ESPC amplitudes. (Right) Summary graphs of decay constants.

(J) β-neurexin KO does not alter the readily releasable vesicle pool as analyzed by stimulation with 0.5 M sucrose. (Left) Representative traces. (Right) Total charge transfer.

Data in (D)–(J) are means ± SEM (numbers of neurons/independent cultures examined are shown in graphs). Statistical analyses were performed by Student's t test (*$p < 0.05$; **$p < 0.01$; ***$p < 0.001$).

See also Figures S1, S2, S3, and S4.

impaired the function of the more strongly endocannabinoid-regulated synapses in the subiculum. The importance of this circuit-specific synaptic alteration emerged from behavioral studies, showing that the β-neurexin KO in the adult CA1 region produced an impairment of contextual fear memory. Thus, β-neurexins are produced as minor transcripts of neurexin genes that nevertheless are essential for the regulation of mammalian synaptic circuits due to modulation of endocannabinoid signaling via an unanticipated trans-synaptic mechanism.

RESULTS

Generation of β-Neurexin-Specific Conditional Triple-KO Mice

Using qRT-PCR, we found that throughout the brain, all three β-neurexins were expressed at levels 10- to 100-fold lower than are corresponding α-neurexins (Figures 1A and S1). Despite their low abundance, however, β-neurexins are highly conserved and might still perform essential functions. To test this hypothesis, we generated conditional and constitutive KO mice of all β-neurexin genes (Figures 1B and S2A–S2C). In these mice, the 5′ exon that encodes the N-terminal β-neurexin-specific sequences was flanked by loxP sites, and epitope tags were inserted into the β-neurexin-specific sequences (EGFP for neurexin-1β and -3β; a hemagglutinin [HA] tag for neurexin-2β). We generated single-, double-, and triple-conditional and constitutive β-neurexin KO mice (see the Experimental Procedures for details) and focused our analyses on triple-mutant mice, targeting all β-neurexins to brace for potential redundancies among β-neurexins.

Conditional triple KO (cKO) mice were viable and fertile. The EGFP and HA tags did not alter expression of either α- or β-neurexin mRNAs (Figures S2D and S2E). Probably because of their low expression levels, tagged β-neurexins could not be detected in total brain extracts, but were readily observed after immunoprecipitations of β-neurexins with EGFP antibodies (Figure 1C).

Constitutive triple-β-neurexin KO mice were also viable but were significantly smaller than wild-type mice and unable to reproduce (Figure S2F). Even single-neurexin-2β and -3β KO mice exhibited a significantly reduced body weight. Thus, β-neurexins—despite low abundance and in contrast to α-neurexins (Missler et al., 2003)—are important for animal health but are not essential for animal survival.

Conditional β-Neurexin KO Impairs Neurotransmitter Release at Excitatory Synapses

We cultured cortical neurons from triple-β-neurexin cKO mice and infected them with lentiviruses expressing active (Cre; to delete all β-neurexins) or inactive, truncated Cre-recombinase (ΔCre; as a control). β-neurexin KO neurons exhibited no change in dendritic arborization or synaptic morphology, suggesting normal neuronal development (Figures 1D, 1E, S3, and S4A–S4E). We evoked action potential-induced excitatory and inhibitory postsynaptic currents (EPSCs and IPSCs, respectively; Kaeser et al., 2011) and separately monitored pharmacologically isolated AMPA-receptor (AMPAR)- and NMDA-receptor (NMDAR)-mediated EPSCs and GABA-receptor (GABAR)-mediated IPSCs. Strikingly, the β-neurexin KO decreased both AMPAR- and NMDAR-mediated EPSCs by ∼50%, but had no effect on GABAR-mediated IPSCs (Figures 1F–1H).

These results suggest that the β-neurexin KO caused a decrease in the probability of glutamate release at excitatory synapses. To directly test this hypothesis, we measured presynaptic release probability using the progressive use-dependent block of evoked NMDAR EPSCs by MK-801 (Hessler et al., 1993; Rosenmund et al., 1993). We observed in triple-β-neurexin KO neurons a robust, ∼2-fold decrease in the rate of synaptic NMDAR inactivation in the presence of MK-801, suggesting an ∼2-fold decrease in release probability (Figure 1I). This decrease was not due to a change in the readily releasable pool of synaptic vesicles because the β-neurexin deletion had no effect on hypertonic sucrose-evoked EPSCs (Figure 1J).

β-Neurexin KO Impairs Action Potential-Induced Ca^{2+} Influx into Presynaptic Terminals

The electrophysiological data suggest that β-neurexins are required for normal coupling at excitatory synapses of an action potential to Ca^{2+}-triggered release, possibly because voltage-gated Ca^{2+} influx is impaired. To test this hypothesis, we constructed a chimeric protein (GCaMP5G-Syb2) containing an N-terminal GCaMP5G Ca^{2+} indicator fused to the synaptic vesicle protein synaptobrevin-2 (Figure 2A). After lentiviral expression in neurons, GCaMP5G-Syb2 was efficiently targeted to presynaptic terminals (Figure 2B). To restrict analyses of presynaptic Ca^{2+} transients to excitatory synapses, we sparsely transfected neurons with mCherry and monitored action potential-elicited Ca^{2+} transients only in presynaptic boutons contacting postsynaptic dendritic spines (Figure 2B). Electrical-field stimulation (1–100 stimuli at 50 Hz) elicited robust Ca^{2+}-induced fluorescence signals in these boutons that saturated after ∼20 stimuli, consistent with accumulation of residual Ca^{2+} in presynaptic terminals during stimulus trains (Figures 2B and 2C). Ca^{2+} signals were blocked by tetrodotoxin (TTX), confirming that they were induced by action potential-stimulated Ca^{2+} influx. For analyses, we normalized the Ca^{2+}-induced fluorescence signals to the maximal fluorescence change induced by 100 stimuli (ΔF_{sat}), which saturates the GCaMP5G-Syb2 Ca^{2+} sensor.

We then used GCaMP5G-Syb2 to analyze Ca^{2+} transients in β-neurexin KO and control neurons. Ca^{2+} influx was induced by 1–10 action potential stimuli in the linear range of our Ca^{2+} sensor (Figure 2C). We found that KO of β-neurexins significantly attenuated action potential-induced Ca^{2+}-transients, with an overall ∼2-fold decrease (Figures 2D and 2E). KO of β-neurexins had no effect on presynaptic levels of voltage-gated N- or P/Q-type Ca^{2+}-channels, suggesting a functional impairment (Figures 2F and S4F–S4H).

Viewed together, these data show that the β-neurexin KO causes a ∼2-fold decrease in three excitatory synapse parameters: EPSC amplitude, release probability, and action-potential-induced Ca^{2+} influx. This suggests that β-neurexins, despite their low abundance compared to α-neurexins, are selectively essential for normal action-potential gated Ca^{2+} influx during neurotransmitter release at excitatory synapses.

β-Neurexin KO Decreases Spontaneous Mini Release at Excitatory Synapses: Selective Rescue by Neurexin-1β Lacking an Insert in SS4

Neurotransmitter release occurs at synapses not only in response to action potentials but also as spontaneous miniature EPSCs (mEPSCs) or miniature IPSCs (mIPSCs) that are largely dependent on intracellular Ca^{2+} (Xu et al., 2009). The β-neurexin KO substantially depressed the mEPSC frequency (∼2-fold), slightly decreased the mEPSC amplitude, and lowered the surface levels of GluA1 AMPARs (Figures 3A, 3B, S4I, and S4J). However, β-neurexin KO had no effect on mIPSC frequency and amplitude (Figures 3C and 3D), consistent with the selective suppression of the presynaptic release probability by the β-neurexin KO in excitatory, but not in inhibitory, synapses.

To validate the specificity of the β-neurexin KO effects on neurotransmitter release, we used "mini" release as a measure of release probability and tested the ability of neurexin-1β containing or lacking an insert in splice site #4 (SS4) and of neurexin-1α lacking an insert in SS4 to rescue the phenotype. Only neurexin-1β lacking an insert in SS4 rescued the decrease in excitatory synaptic transmission in β-neurexin KO neurons (Figures 3E and 3F). Neurexin-1β lacking an insert in SS4 also

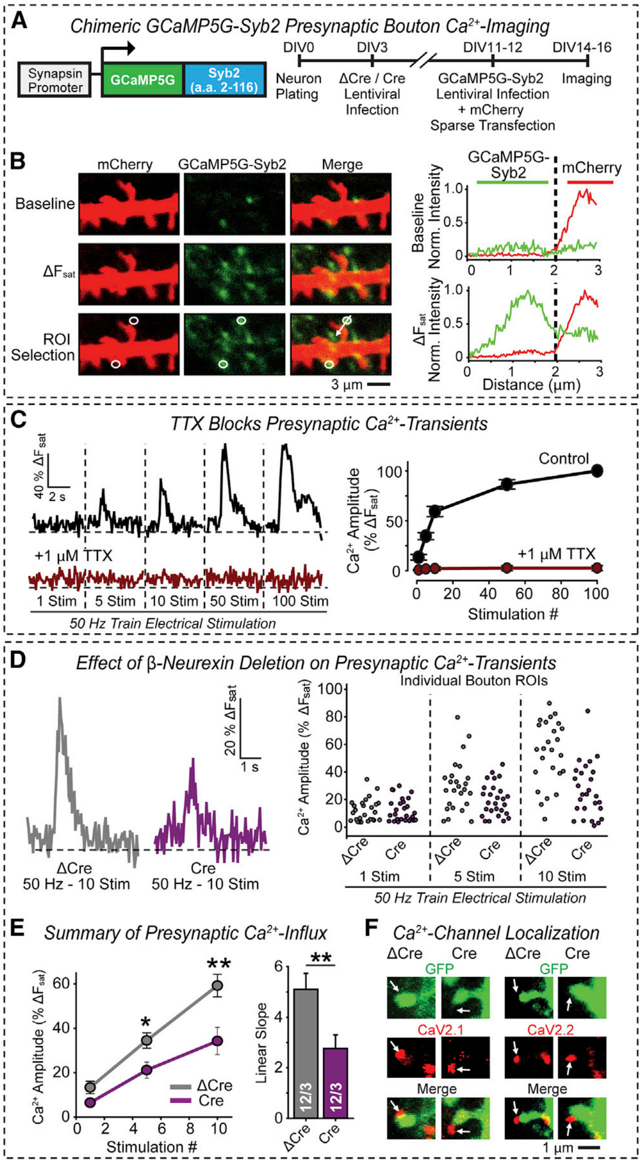

Figure 2. Conditional KO of β-Neurexins Impairs Presynaptic Ca^{2+} Influx

(A) Design of Ca^{2+} imaging experiments. (Left) Schematic of the GCaMP5G-Syb2 fusion protein that acts as a presynaptic Ca^{2+} probe; (Right) Flow diagram of experiments.

(B) Representative Ca^{2+} imaging experiments. (Left) Sample images of presynaptic boutons containing GCaMP5G-Syb2 (green) that contact mCherry-containing dendritic spines (red; images were obtained before and after maximal stimulation to saturate Ca^{2+} transients [ΔF_{sat}]; white circles, regions of interest [ROIs] for quantitative analysis by line scans [arrows]). (Right) Summary graphs of line scans through ROIs at before (top) and after maximal stimulation (ΔF_{sat}; bottom; green, presynaptic Ca^{2+} concentration; red, postsynaptic mCherry signal).

(C) Presynaptic Ca^{2+} transients saturate after 20 stimuli and are blocked by TTX. (Left) Representative Ca^{2+} transients. (Right) Summary graphs (−TTX, n = 12 neurons; +TTX, n = 2 neurons).

(D) β-neurexin KO impairs action potential-induced presynaptic Ca^{2+} influx in cultured cortical neurons (ΔCre = control; Cre = KO). (Left) Representative fluorescence traces of ten stimuli applied at 50 Hz. (Right) Scatter plots of individual bouton responses to 1, 5, and 10 stimuli.

(E) Summary plot of mean Ca^{2+} transients after 1, 5, and 10 stimuli. (Left) n = 3 independent experiments with 2–4 boutons per neuron. (Right) Summary graph of the mean linear slopes fitted through the 1, 5, and 10 stimuli plots.

(F) β-neurexin KO does not alter levels or localization of presynaptic Ca^{2+} channels (representative images of cortical pyramidal neuron spines with sparse GFP expression that are stained for presynaptic P/Q-type [CaV2.1] or N-type [CaV2.2] Ca^{2+} channels). For quantitative analyses, see Figures S4F–S4H.

Data are means ± SEM. Statistical analysis was performed by Student's t test (*p < 0.05; **p < 0.01).

See also Figure S4.

enhanced mEPSC amplitude, probably because this neurexin splice variant stabilizes postsynaptic AMPARs (Aoto et al., 2013). The SS4-dependent rescue of the triple-β-neurexin KO phenotype not only validates its overall specificity but also suggests that β-neurexins control synaptic strength via a specific interaction with postsynaptic ligands that do not bind to α-neurexins. Alternative splicing at SS4 dramatically influences neurexin binding to postsynaptic ligands (Boucard et al., 2005; Chih et al., 2006; Ko et al., 2009; Siddiqui et al., 2010; Uemura et al., 2010; Matsuda and Yuzaki, 2011). Indeed, we observed that at least some neuroligin-1 splice variants specifically bind only to β-neurexins, but not to α-neurexins lacking an insert in SS4 (Figure S5I).

β-Neurexin KO Enhances Basal Endocannabinoid Activity

How might deletion of β-neurexins influence presynaptic Ca^{2+} influx? A hint derives from the synaptic dysfunction caused by the neuroligin-3 KO, a postsynaptic cell-adhesion molecule that binds to presynaptic neurexins (Südhof, 2008). In CA1 pyramidal neurons, the neuroligin-3 KO decreases tonic endocannabinoid signaling, mediated by cannabinoid receptor type 1 (CB1R), at inhibitory synapses from CCK-positive basket neurons, thereby increasing GABA release (Földy et al., 2013). This observation led us to ask whether the β-neurexin KO might cause the opposite change at excitatory synapses, i.e., an increase in basal endocannabinoid signaling, that could account for the decrease in Ca^{2+} influx and neurotransmitter release in β-neurexin KO synapses.

We tested the effect of the CB1R antagonist AM251 on mEPSCs, again used as a measure of presynaptic release probability. AM251 had no effect on the mEPSC amplitude or frequency in control neurons (Figures 3G and S5A–S5D). However, AM251 significantly enhanced the mEPSC frequency without changing the mEPSC amplitude in β-neurexin KO neurons (Figures 3G and S5A–S5D), suggesting that KO of β-neurexins enhances basal endocannabinoid tone.

To further explore this hypothesis, we examined the effects of the CB1R agonist WIN (WIN55,212-2 mesylate) on mEPSCs. While WIN produced a similar relative decrease in mEPSC frequency in triple-β-neurexin KO and control neurons (Figure S5G), we observed a significantly smaller absolute decrease in mEPSC frequency in KO neurons (Figures 3H and S5H). This observation, consistent with the findings from the AM251 experiments, suggests that in β-neurexin KO synapses, CB1Rs are partially activated, and thus less additional inhibition is induced by WIN. Together, these data indicate that the β-neurexin KO caused an increase in the basal activity of presynaptic CB1Rs, which are known to inhibit presynaptic Ca^{2+} channels and to decrease neurotransmitter release (Twitchell et al., 1997; Kreitzer and Regehr, 2001; Brown et al., 2004; Szabó et al., 2014). Consistent with observations on neuroligin-3 (Földy et al., 2013), these data reveal a connection of the neurexin/neuroligin complex to endocannabinoid signaling. The direction of the effects, however, is diametrically opposite: whereas the β-neurexin KO suppresses the presynaptic neurotransmitter release probability at excitatory synapses, the neuroligin-3 KO increases release at inhibitory synapses.

Conditional β-Neurexin KO Increases Postsynaptic 2-AG Synthesis

To begin to explore how the β-neurexin KO increases the basal endocannabinoid "tone" at excitatory synapses, we examined CB1R levels in β-neurexin KO neurons by immunoblotting and immunocytochemistry. We detected no changes, suggesting that presynaptic β-neurexins may influence endocannabinoid synthesis, which is postsynaptic (Figures 4A–4D; Murataeva et al., 2014, Castillo et al., 2012, Di Marzo et al., 2004). To test which of the brain's two major endocannabinoids—2-AG and anandamide—is active at the synapses that are affected by the β-neurexin KO, we measured the effects of exogenous 2-AG and anandamide on mEPSCs in control and β-neurexin KO neurons.

Bath-applied anandamide had only a modest effect on mEPSCs in cultured cortical neurons, with no significant difference between control and β-neurexin KO neurons. In contrast, 2-AG robustly suppressed mEPSC frequency in control neurons, but not in β-neurexin KO neurons (Figures 4E and 4F). This observation, consistent with the findings from the AM251 and WIN experiments (Figures 3G and 3H), suggests that the β-neurexin KO partially activates CB1Rs by increasing basal levels of 2-AG, which prevents the additional inhibition by exogenous 2-AG. Anandamide is likely relatively inactive because it is a partial agonist and may not primarily act via CB1Rs (Freund et al., 2003).

2-AG is synthesized via a postsynaptic phospholipase C-dependent pathway (Figure 4A). To test whether postsynaptic 2-AG synthesis may be upregulated upon loss of presynaptic β-neurexins, we blocked phospholipase C-dependent 2-AG synthesis specifically in postsynaptic neurons by introducing the phospholipase C inhibitor U73122 via the patch pipette into postsynaptic neurons. U73122 had only minimal effects in control neurons, but caused full rescue of the mEPSC frequency in β-neurexin KO neurons (Figure 4G).

Together, these data suggest that increased postsynaptic 2-AG synthesis produces the presynaptic β-neurexin KO phenotype. To

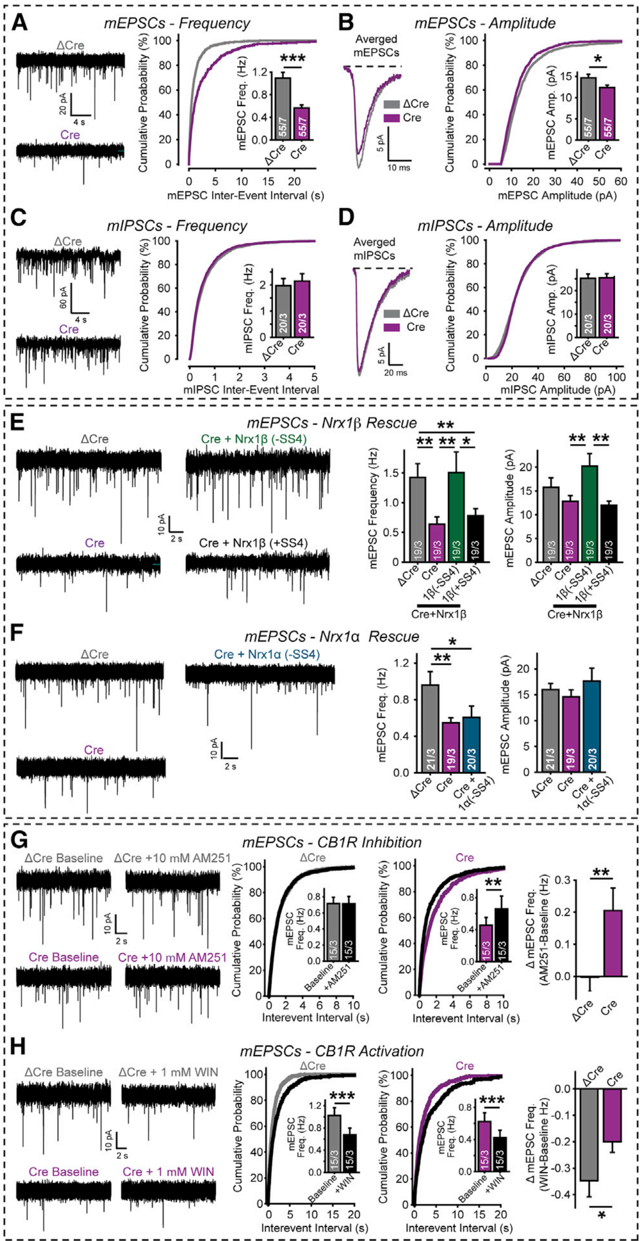

Figure 3. Neurexin-1β, but Not Neurexin-1α, and the CB1R Antagonist AM251 Rescue Impaired Spontaneous Mini Release in β-Neurexin KO Neurons

(A–D) β-neurexin KO impairs mini release at excitatory, but not inhibitory, synapses (A and B, mESPCs; C and D, mIPSCs) in cortical neurons from triple-β-neurexin cKO mice expressing inactive (ΔCre) or active Cre-recombinase (Cre). (A and C) Representative traces (left), cumulative distributions of inter-event intervals (right), and mean event frequencies (inset). (B and D) Average individual events (left), cumulative distributions of event amplitudes (right), and mean event amplitudes (inset).

(E) Neurexin-1β without an insert in SS#4 (–SS4), but not with an insert (+SS4), rescues the decreased mEPSC frequency in β-neurexin KO neurons.

(F) Neurexin-1α without an insert in SS#4 (–SS4) fails to rescue the decreased mEPSC frequency in β-neurexin KO neurons.

(G) Blocking CB1Rs with AM251 reverses the decrease in mEPSC frequency in β-neurexin KO neurons. (Left) Representative traces. (Center) Cumulative distributions of event frequencies with insets showing mean frequencies; (Right) Summary graphs of AM251-induced changes.

(H) Activating CB1Rs with WIN (WIN 55,212-2 mesylate) depresses mini release significantly more in control (ΔCre) than in β-neurexin KO neurons (Cre). The figure design is analogous to that of (G).

Data are means ± SEM; the numbers of neurons/independent cultures examined are shown in the graphs. Statistical analyses were performed using Student's t test (*$p < 0.05$; **$p < 0.01$; ***$p < 0.001$).

See also Figures S4 and S5.

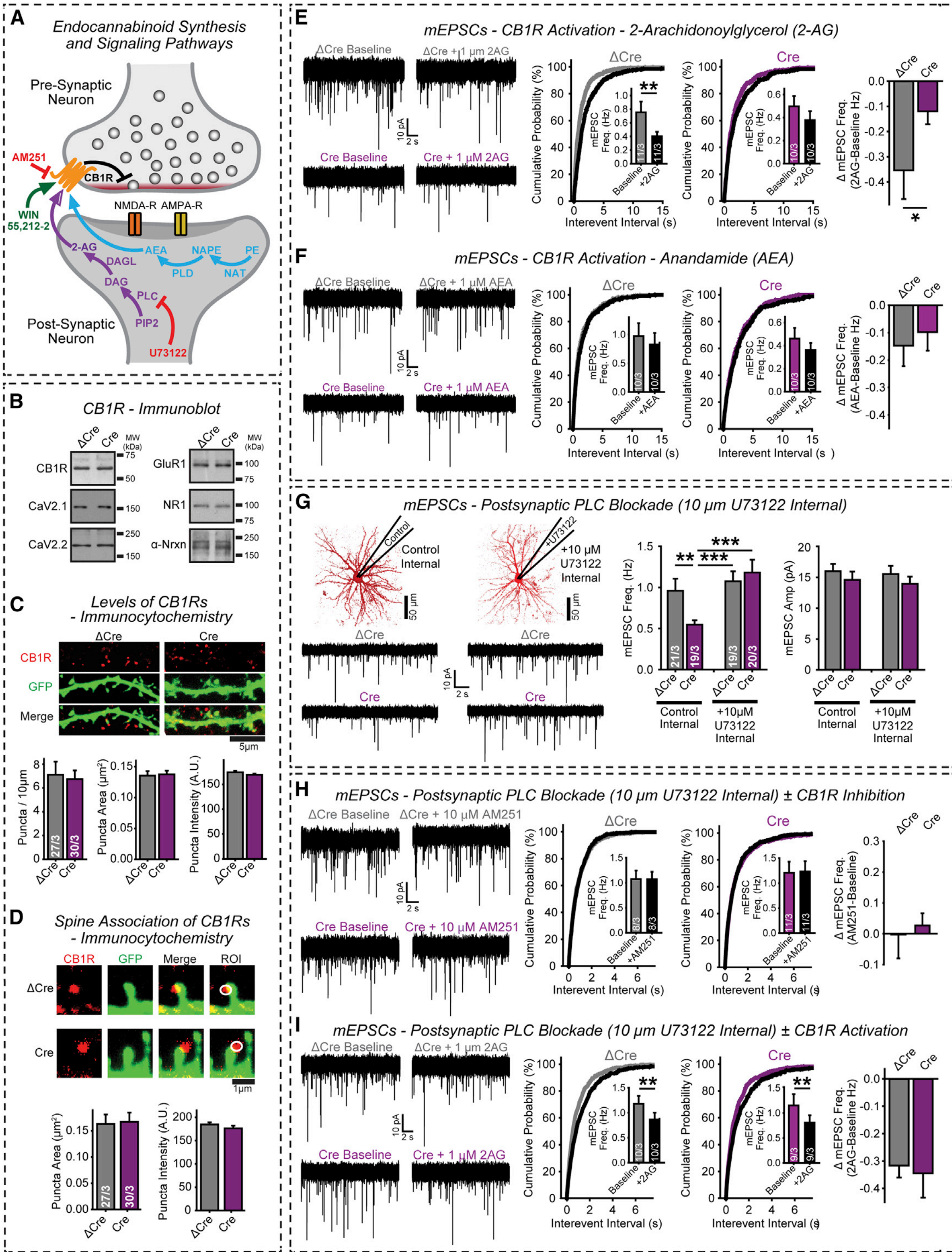

Figure 4. Blocking Postsynaptic 2-AG Synthesis Rescues Presynaptic β-Neurexin KO Phenotype in Cultured Neurons

(A) A diagram of endocannabinoid signaling pathways. Two distinct endocannabinoids (2-arachidonoylglycerol [2-AG] and anandamide [AEA, N-arachidonoylethanolamine]) are synthesized by different postsynaptic enzymes; both act on presynaptic CB1Rs (PLC, phospholipase C; PIP2, phosphatidylinositol 4,5-bisphosphate; DAG, diacylglycerol; DAGL, diacylglycerol lipase; NAT, N-acyltransferase; PE, phosphatidylethanolamine; NAPE, *N*-arachidonoyl phosphatidylethanolamine; PLD, phospholipase D). Modes of action of the 2-AG synthesis inhibitor U73122 and the CB1R agonist WIN and antagonist AM251 are indicated.

(legend continued on next page)

consolidate this conclusion, we assayed the state of CB1Rs as a function of postsynaptic 2-AG synthesis inhibition. We bath-applied the CB1R-antagonist AM251 (Figure 4H) or the CB1R-agonist 2-AG (Figure 4I), while recording from postsynaptic neurons containing the 2-AG synthesis inhibitor U73122. U73122 eliminated the enhanced basal activity of CB1Rs in β-neurexin KO neurons (Figures 3G and 4H) and restored the sensitivity of CB1Rs to exogenous 2-AG (Figures 4F and 4I). Thus, postsynaptic inhibition of 2-AG synthesis in β-neurexin KO neurons restores the signaling set-point of presynaptic CB1Rs to that observed in control neurons, confirming that β-neurexins activate presynaptic CB1Rs via an upregulation of postsynaptic 2-AG synthesis.

Conditional β-Neurexin KO In Vivo Suppresses Release at Hippocampal Output Synapses

Modulation of endocannabinoid signaling by β-neurexins would have significant circuit implications and could be relevant not only for understanding abnormalities of circuit dynamics in neuropsychiatric disorders but also for possible future therapeutic options. Thus, we tested whether β-neurexins also control endocannabinoid signaling in vivo.

We stereotactically injected AAVs encoding Cre-EGFP or ΔCre-EGFP into the hippocampal CA1 region of triple-β-neurexin cKO mice at P21 and analyzed acute subiculum slices at P35–P40 (Figure 5A). We monitored synaptic transmission at synapses formed by CA1-region axons onto pyramidal neurons of the subiculum, which is the major output pathway of the hippocampus. In this approach, only presynaptic neurons are genetically manipulated (Aoto et al., 2013). Pyramidal subiculum neurons comprise two broad classes—"regular-firing" and "burst-firing" neurons—that can be readily distinguished by the pattern of action potentials induced by current injections (Figure 5B; Graves et al., 2012; Staff et al., 2000; van Welie et al., 2006). All analyses were performed separately in these two classes of neurons. Upon whole-cell break-in, we identified the neuron type in current-clamp mode and then recorded EPSCs induced by stimulating CA1-region axons in voltage-clamp mode (Figure 5B).

We assessed excitatory synaptic strength by measuring the input-output relationship (Figures 5C and 5D). In regular-firing neurons, the β-neurexin KO produced a trend toward decreased synaptic strength (Figure 5C). In burst-firing neurons, however, the β-neurexin KO caused a ~2-fold decrease in synaptic strength, similar to cultured cortical neurons (Figure 5D). Moreover, we measured paired-pulse ratios (PPRs) that inversely correlate with the presynaptic release probability (Kaeser and Regehr, 2014). Again, the presynaptic β-neurexin KO caused no change in regular-firing neurons (Figure 5E), but increased the PPR in burst-firing neurons, consistent with a decrease in release probability (Figure 5F). Thus, the presynaptic β-neurexin KO selectively decreases neurotransmitter release in burst-firing neuron synapses.

β-Neurexins Control Endocannabinoid Regulation of Subiculum Synapses

Does the presynaptic β-neurexin KO impair neurotransmitter release in burst-firing subiculum neuron synapses by an endocannabinoid-dependent mechanism similar to cultured cortical neurons? To address this question, we first needed to learn whether tonic endocannabinoid signaling normally regulates release at subiculum synapses. Bath application of the CB1R antagonist AM251 had no effect on EPSC amplitudes in regular-firing neurons, but caused a significant enhancement of EPSCs in burst-firing neurons (Figure 5G). Bath application of the CB1R agonist WIN, conversely, induced a modest depression of EPSCs in regular-firing neurons but a significantly stronger depression of EPSCs in burst-firing neurons (Figure S6A). Thus, endocannabinoids tonically modulate excitatory synapses formed onto burst-firing neurons and perform a smaller role at synapses formed onto regular-firing neurons.

Next, we explored whether the β-neurexin KO decreases neurotransmitter release in burst-firing neuron synapses by increasing basal endocannabinoid tone. To this end, we bath-applied AM251 to subiculum slices without or with presynaptic KO of β-neurexins. Presynaptic β-neurexin KO caused a significant increase in the AM251-dependent enhancement of EPSCs (Figure 5H), suggesting that similar to cultured neurons in vitro (Figure 3G), the β-neurexin KO increased endocannabinoid-dependent inhibition of release in burst-firing neuron synapses in vivo (Figure 5H). The β-neurexin KO did not change the relative magnitude of the EPSC depression by WIN (Figures S5G and S6B), likely because the enhanced basal CB1R activity is not saturated by loss of β-neurexins. Together, these findings suggest that the β-neurexin KO decreases excitatory synaptic strength in burst-firing subiculum neurons, at least in part, by enhancing tonic activation of CB1Rs in presynaptic terminals of CA1 pyramidal neurons.

(B–D) CB1R levels are similar in cortical neurons from triple-β-neurexin cKO mice expressing inactive (ΔCre) or active Cre-recombinase (Cre). (B) Representative immunoblots with antibodies to CB1R, CaV2.1, and CaV2.2 Ca^{2+} channels, GluR1, NR1 (an NMDAR subunit), and α-neurexins. (C and D) Immunocytochemistry quantifications of CB1R levels (C) and CB1R localization (D). Note that neurons were sparsely transfected with EGFP for visualization of neuronal morphology.
(E and F) 2-AG causes a larger depression of mini release in control than in β-neurexin KO neurons (E), whereas anandamide is ineffective likely because it is only a partial agonist (F). (Left) Representative traces. (Center) Cumulative distributions of mEPSC inter-event intervals (insets = mean frequencies). (Right) Summary graphs of anandamide- or 2-AG-induced changes.
(G) Selective postsynaptic block of 2-AG synthesis by U73122 in the patch pipette rescues decreased mini release in β-neurexin KO neurons. (Left) Experimental setup and representative mEPSC traces. (Right) Bar diagrams of mEPSC frequencies and amplitudes.
(H and I) Selective postsynaptic block of 2-AG synthesis by U73122 prevents CB1R activation in β-neurexin KO neurons as measured by blocking CB1Rs with bath-applied AM251 (H) or activating CB1Rs with bath-applied 2-AG (I). (Left) Representative traces. (Center) Cumulative distributions of mEPSC inter-event intervals (insets = mean frequencies). (Right) Summary graphs of AM251- or 2-AG-induced changes in mEPSC frequencies.
Data are means ± SEM; the numbers of neurons/independent cultures examined are shown in graphs. Statistical analyses were with Student's t test (*$p < 0.05$, **$p < 0.01$, ***$p < 0.001$).
See also Figure S5.

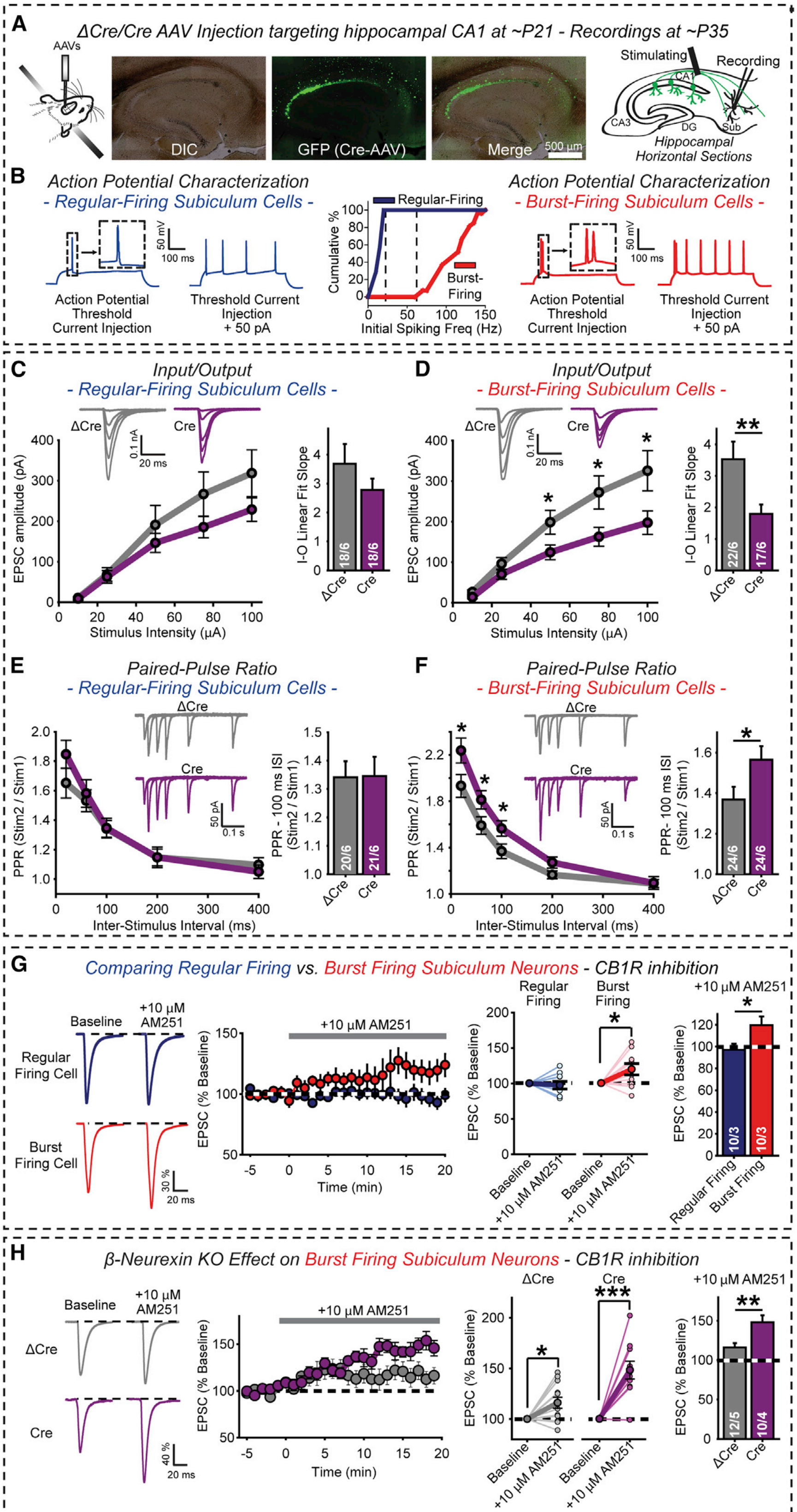

Figure 5. Presynaptic KO of β-Neurexins in CA1 Pyramidal Neurons Decreases Synaptic Strength at Burst-Firing Neuron Synapses in the Subiculum

(A) Experimental design. (Left) Diagram of stereotactic injections into the CA1 region. (Center) Representative images of slices from stereotactically injected mice at P35 to visualize AAV infections (slices with <90% EGFP expression in the CA1 region were rejected). (Right) Electrophysiological recording configuration in acute subiculum slices (Aoto et al., 2013).

(B) Identification of regular- and burst-firing pyramidal subiculum neurons in current-clamp mode. (Left and Right) Representative traces. (Center) Summary graph of the initial spiking frequency.

(C and D) Input/output (I/O) relations of AMPAR-mediated EPSCs elicited by stimulation of CA1-derived axons and recorded in regular- (C) or burst-firing subiculum neurons (D). (Left) Summary plots with representative traces on top. (Right) Summary graphs of fitted linear input/output slopes.

(E and F) Paired-pulse ratio (PPR) measurements of AMPAR EPSCs in regular- (E) and burst-firing subiculum neurons (F). (Left) Summary plots of PPRs versus inter-stimulus intervals with representative traces on top. (Right) Summary graphs of PPRs at 100-ms inter-stimulus intervals.

(G) Only burst-firing, but not regular-firing, subiculum neurons exhibit tonic endocannabinoid signaling in wild-type mice. EPSCs were elicited at 0.1 Hz before and after bath application of the CB1R antagonist AM251. (Left) Representative EPSC traces. (Center) Plots of relative EPSC amplitudes and AM251-induced EPSC amplitude changes in individual neurons. (Right) Summary graphs of AM251-induced EPSC amplitude changes.

(H) Presynaptic β-neurexin KO increases tonic endocannabinoid signaling in burst-firing subiculum neurons. Experiments were performed as in (G), except that burst-firing neurons were analyzed in slices from β-neurexin cKO mice with presynaptic expression of ΔCre- or Cre-EGFP in the CA1 region (see A).

Data are means ± SEM; the numbers of neurons/mice examined are shown in the summary graphs. Statistical analysis was by paired Student's t test for single-cell plots and unpaired Student's t test for comparisons in other summary graphs (*p < 0.05; **p < 0.01; ***p < 0.001).

See also Figure S6.

β-Neurexins Control Long-Term Plasticity in Burst-Firing Neuron Synapses

In regular-firing neurons of the subiculum, LTP is induced by postsynaptic activation of NMDARs, whereas in burst-firing neurons LTP is induced by presynaptic activation of PKA (Wozny et al., 2008; Behr et al., 2009). We asked whether LTP may also be differentially affected by the presynaptic β-neurexin KO in regular- and burst-firing neurons, similar to endocannabinoid signaling. We observed no effect of the β-neurexin KO on LTP in regular-firing neurons (Figure 6A). Strikingly, however, the β-neurexin KO blocked LTP in burst-firing neurons (Figure 6B).

Presynaptic LTP in burst-firing neurons depends on adenylate cyclase/PKA signaling (Wozny et al., 2008). Interestingly, CB1Rs are coupled to $G\alpha_i$, which inhibits adenylate cyclase (Castillo et al., 2012; Kano et al., 2009). Thus, we hypothesized that enhanced basal CB1R activity caused by the β-neurexin KO may contribute to, or even cause, the LTP impairment. To test this hypothesis, we examined the effects of AM251 on LTP in burst-firing subiculum neurons. AM251 had no effect on LTP in control neurons (Figure 6C), but rescued the blocked LTP in β-neurexin KO neurons (Figure 6D). To examine whether the mechanism of CB1R activation by the β-neurexin KO in LTP mirrors that of CB1R activation in release, we asked whether postsynaptic inhibition of 2-AG synthesis also rescued the LTP impairment in β-neurexin KO synapses. Indeed, selective introduction of the 2-AG synthesis inhibitor U73122 into postsynaptic patched neurons (Figure 4A) had no effect on LTP in control slices but fully rescued the block of LTP in β-neurexin KO slices (Figures 6E and 6F). These results suggest that following the genetic ablation of β-neurexins, tonic postsynaptic 2-AG synthesis is enhanced and activates presynaptic CB1Rs, which impair this form of LTP.

Deletion of β-Neurexins in CA1 Region Neurons Impairs Contextual Fear Memory

To examine whether the function of β-neurexins in hippocampal CA1 neurons is important for learning and memory, we tested the behavioral effects of deleting β-neurexins from the hippocampal CA1 region (Figures 7A and 7B). We observed no changes in the open-field behavior of mice, as measured quantitatively on a force actometer (Figures 7C and S7A). We then performed simultaneous cued and contextual fear conditioning. The CA1-region-specific β-neurexin KO did not impair fear-learning acquisition (Figure S7B), but strongly reduced freezing behavior when the mouse was placed in the context of the tone-foot-shock pairings (Figure 7D). This phenotype was specific for contextual memory since the β-neurexin KO had no effect on freezing in response to an altered context or to the auditory cue, indicating that contextual fear memory—which is known to be dependent on hippocampal function (Fanselow and Dong, 2010)—is selectively impaired by the β-neurexin KO (Figure 7D).

DISCUSSION

We analyzed triple-conditional KO mice that target all β-neurexin genes in two preparations: cultured cortical neurons after conditional KO of β-neurexins in vitro, and acute subiculum slices after conditional presynaptic KO of β-neurexins in vivo. Our data demonstrate that β-neurexins regulate the strength and long-term plasticity of a subset of excitatory synapses, that the β-neurexin KO impairs presynaptic Ca^{2+} influx triggered by an action potential in these synapses, and that presynaptic β-neurexins control tonic postsynaptic endocannabinoid signaling mediated by 2-AG (Figure 7D). Our in vivo results further suggest that β-neurexins regulate neural circuits by modulating the strength and plasticity of a subset of excitatory synapses via endocannabinoids and that this regulation is behaviorally important. Given the complex nature of the many overlapping neural circuits that ultimately guide behavior, it is perhaps not surprising that the endocannabinoid-dependent modulation of synaptic circuits is controlled by trans-synaptic cell-adhesion molecules, and that this control is essential for the information processing capacity of the brain. However, it is unexpected that β-neurexins as relatively minor neurexin gene transcripts perform a pervasive regulatory role in synapses, a role that adds to previously defined other functions of neurexins (Missler et al., 2003; Aoto et al., 2013, 2015).

In cultured cortical neurons in vitro, KO of β-neurexins decreased the release probability at excitatory synapses ~2-fold by causing a ~2-fold decrease in presynaptic Ca^{2+} transients (Figures 1F–1J, 2D, 2E, and 3A–3D). The magnitude of this effect was surprising considering the low expression of β-neurexins (Figure 1A) and the continued presence of the more abundant α-neurexins. The underlying mechanism consisted, at least in part, of an increase in tonic 2-AG endocannabinoid signaling, as evidenced by the reversal of the release phenotype, both by bath-application of the CB1R-antagonist AM251 (Figure 3G) and by postsynaptic inhibition of 2-AG synthesis (Figure 4G). Thus, β-neurexins appear to be selectively essential for regulating excitatory synaptic strength via a control of tonic endocannabinoid signaling.

In synapses formed by CA1-region pyramidal neurons onto pyramidal neurons in the subiculum in vivo, the β-neurexin KO also impaired excitatory synaptic transmission. We separately examined synapses of regular- and burst-firing neurons, the two types of subiculum pyramidal neurons (Staff et al., 2000; van Welie et al., 2006). The presynaptic β-neurexin KO produced a decrease of excitatory synaptic strength in postsynaptic burst-firing, but not regular-firing, neurons; this loss was reversed, at least in part, by the CB1R antagonist AM251 (Figure 5). Moreover, only PKA-dependent presynaptic LTP in burst-firing, but not NMDAR-dependent postsynaptic LTP in regular-firing, neurons was impaired by the β-neurexin KO (Figures 6A and 6B). Presynaptic LTP in presynaptic β-neurexin KO slices was restored by inhibiting CB1Rs (Figures 6C and 6D) and, most importantly, by postsynaptic inhibition of 2-AG synthesis in burst-firing neurons (Figures 6E and 6F). The regulatory function of presynaptic β-neurexins in release is likely physiologically important since the β-neurexin KO in the CA1 region severely impaired contextual fear conditioning (Figure 7).

To the best of our knowledge, our findings represent the first description of trans-synaptic control of endocannabinoid signaling by neurexins, complementing previous observations of a role of postsynaptic neuroligin-3 in regulating the endocannabinoid tone (Földy et al., 2013). Tonic endocannabinoid signaling at excitatory synapses has not previously been

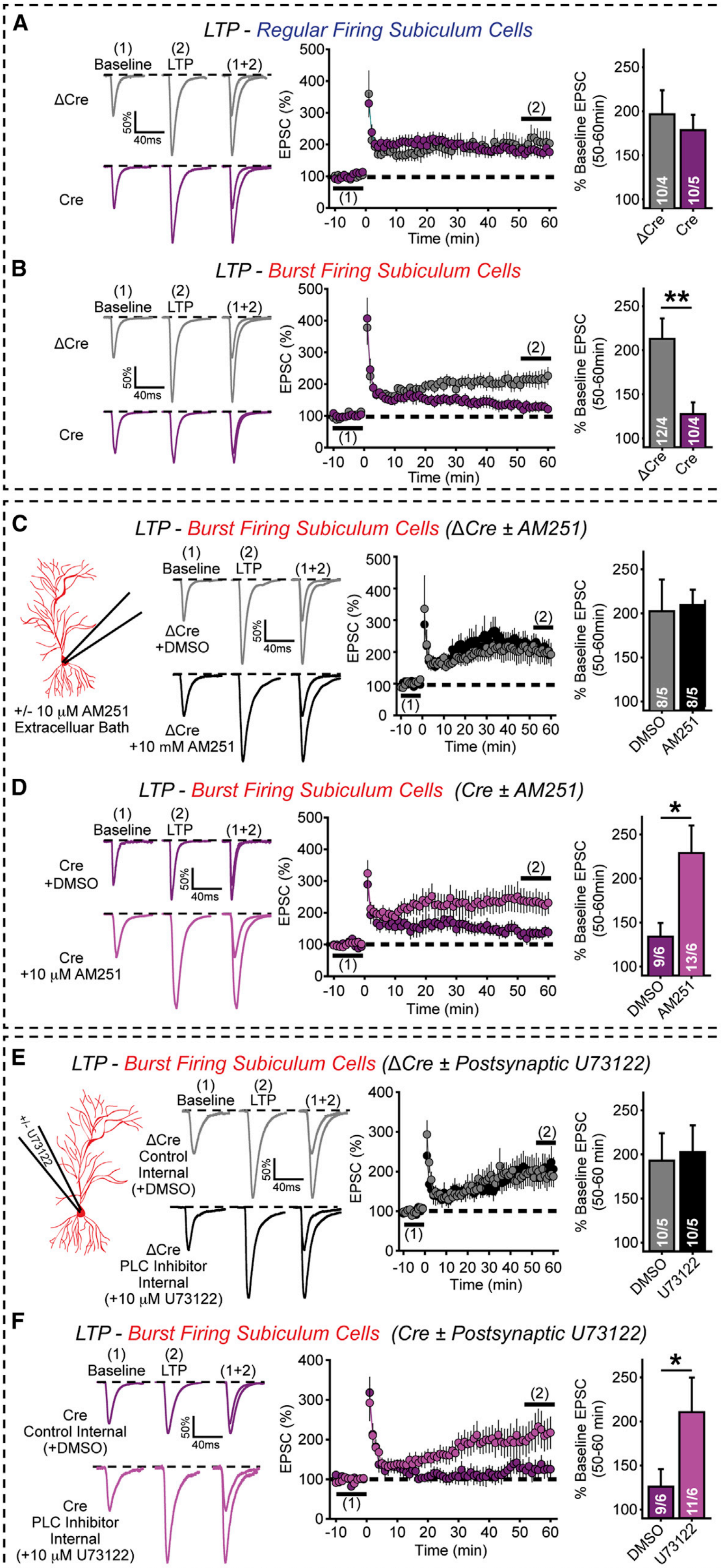

Figure 6. Presynaptic KO of β-Neurexins Selectively Impairs LTP at Burst-Firing Subiculum Neurons by Enhancing Basal Endocannabinoid Activity

(A) KO of β-neurexins does not change LTP of CA1 EPSCs onto regular-firing subiculum neurons. LTP was induced by 4 × 100 Hz/1 s stimulation with 10-s intervals in current-clamp mode at resting potential in acute slices from CA1-region-specific β-neurexin KO mice obtained as described in Figure 5A. (Left) Representative traces. (Center) Average EPSC amplitudes (1-min bins). (Right) Summary graphs of mean LTP magnitude 50–60 min after induction.

(B) Same as in (A), except that burst-firing subiculum neurons were analyzed.

(C and D) Same as in (B), except that the effect of the CB1R antagonist AM251 on LTP was examined in slices from mice injected with inactive Cre-recombinase (C) or with active Cre-recombinase (D).

(E and F) Same as in (C) and (D), except that the effect of the phospholipase C inhibitor U73122 introduced into the postsynaptic neuron via the patch pipette was examined.

Data shown are means ± SEM; numbers of neurons/mice examined are shown in the graphs. Statistical analysis was performed by Student's t test (*p < 0.05; **p < 0.01).

documented, but anatomical evidence supports the presence of DGL-α (which synthesizes the endocannabinoid 2-AG; Figure 4A) and of CB1Rs at excitatory spine synapses in the hippocampus (Katona et al., 2006; Kawamura et al., 2006). Moreover, several studies showed that the CB1R-agonist WIN inhibits extracellular stimulation-evoked glutamate release onto CA1 pyramidal neurons (Hajos et al., 2001; Ohno-Shosaku et al., 2002; Kawamura et al., 2006; Takahashi and Castillo, 2006). Excitatory synapses onto CA1 pyramidal neurons exhibit evidence of phasic, but not tonic, endocannabinoid signaling (Ohno-Shosaku et al., 2002; Földy et al., 2013), suggesting that the regulation of tonic 2-AG signaling by β-neurexins is synapse-specific and further emphasizing how the identity of trans-synaptic neurexin complexes can dictate function. No previous evidence has linked endocannabinoid signaling to modulation of presynaptic LTP of excitatory synapses, although CB1R activation has been implicated in LTD (Peterfi et al., 2012; Han et al., 2012).

Mechanistically, the large effects of the β-neurexin KO in the presence of the more abundant α-neurexins (Figures 1A and S1) suggest that β-neurexins perform unique non-redundant functions. The presynaptic action of β-neurexins (Figures 5 and 6), the SS4-dependence of the rescue (Figure 3E), and the rescue of the presynaptic β-neurexin KO phenotype by blocking postsynaptic synthesis of 2-AG (Figures 4 and 6) demonstrate that the functions of β-neurexins involve trans-synaptic ligand interactions. It is intriguing that some splice variants of neuroligin-1 only bind to β-neurexins, but not to α-neurexins (Figure S5I), and that deletion of neuroligin-3 abolishes tonic endocannabinoid signaling at inhibitory synapses of CCK basket cells (Földy et al., 2013). Although the β-neurexin KO led to the opposite effect at excitatory synapses on subiculum burst-firing neurons, namely, an enhancement of basal endocannabinoid signaling, it is possible that they are due to the same principal process: trans-synaptic regulation of endocannabinoid signaling that involves interactions of specific neurexin splice-variants with particular neuroligin isoforms. Alternatively, it is possible that as yet unknown β-neurexin-specific ligands mediate their functions, or that α- and β-neurexins are localized to distinct synaptic sites in a neuron.

The β-neurexin KO phenotype resembles that of neurexin-3 SS4 knockin mice in that both genetic manipulations reveal a requirement for neurexins lacking an insert in SS4 (Figure 3E; Aoto et al., 2013). However, the phenotypes of these mutations are very different. While the β-neurexin KO caused a decrease in presynaptic release probability and a loss of presynaptic LTP without changes in postsynaptic parameters, the opposite was observed in SS4 knockin mice expressing neurexin-3 with constitutively spliced-in SS4 (Aoto et al., 2013). This difference in phenotypes is likely due to the fact that the SS4 knockin affects all α- and β-transcripts of ONE particular neurexin gene, whereas the β-neurexin triple KO affects all β-transcripts, but not α-transcripts, of all neurexin genes (which primarily express α-neurexins). Thus, the only overlap between the two genetic manipulations involves relatively small amounts of neurexin-3β mRNAs. Any phenotypic overlap of these manipulations likely would have been occluded by their more dramatic general phenotypes, although the small decrease in mEPSC amplitude and AMPAR surface levels in β-neurexin KO synapses (Figures 3A and S4F) may be due to the mechanism described by Aoto et al. (2013) for the neurexin-3 SS4 knockin.

Independent of the molecular mechanism underlying the selective functional role of β-neurexins in regulating excitatory synaptic strength, this role likely has significant implications for neural circuit dynamics (Figures 7A–7D). Information processing by neural circuits involves continuous modulation of synaptic strength at specific sites, such that the input/output relations of a circuit depend on how action potentials are transformed into synaptic signals that eventually cause firing—or inhibition of firing—of the circuit output neurons. Endocannabinoids have emerged as major regulators of circuit dynamics (Katona and Freund, 2008; Castillo et al., 2012; Melis et al., 2014). Thus, the control of endocannabinoid signaling by trans-synaptically acting β-neurexins, which in turn are regulated by alternative splicing, likely impacts circuit dynamics in many brain regions. Understanding such dynamics will be essential for understanding behavior in general, and the conditional β-neurexin KO mice provide a useful tool for region-specific modulation of circuit dynamics in order to probe its behavioral relevance.

EXPERIMENTAL PROCEDURES

In all experiments, the researcher was blinded to the genetic manipulation. All plasmids are available upon request, and the mice described here were deposited in Jackson Labs for distribution. Brief experimental procedures are listed here. For details, please see the Supplemental Experimental Procedures.

Mouse Generation and Husbandry

Neurexin-β-floxed (NBF) mice were generated by homologous recombination targeting the 5′ unique exon for each of the three β-neurexin genes that is not shared with its α-neurexin counterparts. All procedures conformed to NIH Guidelines for the Care and Use of Laboratory Animals and were approved by the Stanford University Administrative Panel on Laboratory Animal Care.

mRNA Measurements

mRNA measurements were performed using qRT-PCR on RNA isolated from ∼P30 mouse brain tissues using the RNAqueous-Micro RNA Isolation Kit (Invitrogen). Reactions for α- and β-neurexins and GAPDH (internal control) were run with primers and probes as described in the Supplemental Experimental Procedures.

Neuron Cultures

Cortical neurons were cultured from newborn NBF mice, infected on DIV 3–4 with lentiviruses, transfected using the calcium phosphate method when indicated, and analyzed at DIV 14–16.

Virus Preparations

Nuclear localized EGFP-Cre and EGFP-ΔCre fusion proteins deliverable by lentiviruses were from previously described vectors (Kaeser et al., 2011). All neurexin-1β rescue constructs were previously described mouse cDNAs expressed from separate lentiviruses (Aoto et al., 2013). For in vivo infections, we employed an AAV-DJ strain that is highly efficient in vivo as previously described (Xu et al., 2012).

Stereotactic Injections

Stereotactic injections of AAVs were performed as previously described (Xu et al., 2012). Efficiency and localization of AAV expression were confirmed by fluorescence of nuclear EGFP encoded by the expressed inactive and active EGFP-Cre-recombinase fusion proteins.

Ca^{2+} Imaging

A chimeric GCaMP5G-Syb2 was made and used in order to target GCaMP5G calcium sensor to presynaptic terminals as described in the Supplemental

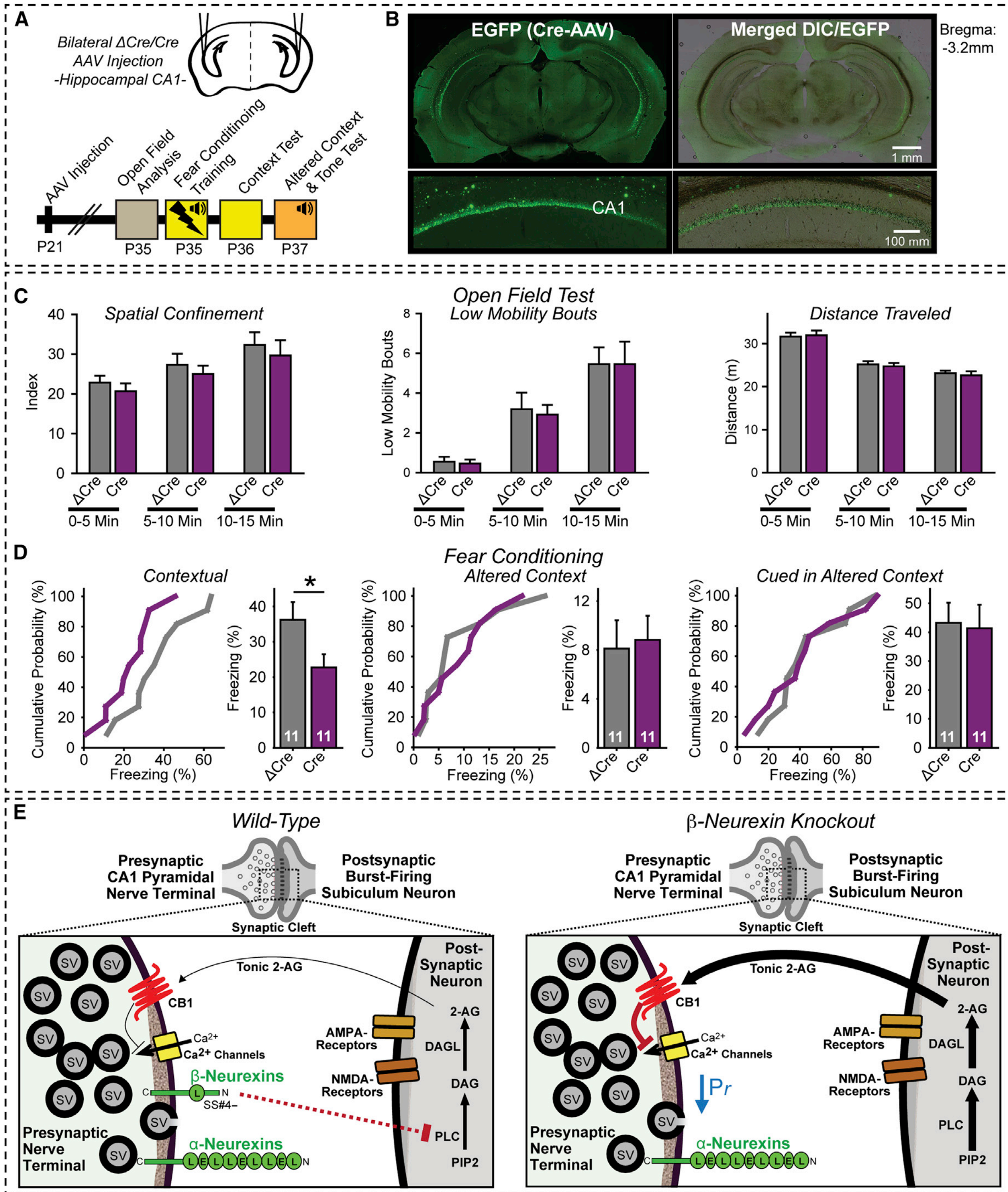

Figure 7. Conditional KO of β-Neurexins in the Hippocampal CA1 Region Impairs Contextual Memory: Model for β-Neurexin Action

(A) Design of behavioral experiments following Xu et al. (2012).

(B) Representative coronal images illustrating expression of Cre-EGFP in the CA1 region of the hippocampus after stereotactic injection (top) and zoomed CA1 image (bottom).

(C and D) Analysis of ΔCre- or Cre-injected mice in open-field (C) and fear conditioning tests (D). Open-field behavior (analyzed in three 5-min segments) was quantified as spatial confinement (C, left), low-mobility bouts (C, center), and total distance traveled (C, right). Fear conditioning training exposed mice to three 30-s tones ending with 2-s electrical foot shocks separated by 1-min intervals (D; left, graphs, cumulative distributions; right, summary graphs, mean fear conditioning memory as measured by freezing). Data are means ± SEM; the numbers of mice examined are shown in the graphs. Statistical analysis was performed by Student's t test (*$p < 0.05$).

(legend continued on next page)

Experimental Procedures. Neuronal morphology was visualized by sparse Ca^{2+}- phosphate transfection with mCherry expression construct, and imaging was performed on a Zeiss LSM 510 confocal microscope.

Electrophysiology

For details of electrophysiological recordings from cultured neurons and acute slices, see the Supplemental Experimental Procedures.

Fear Conditioning

Fear conditioning and open-field behavioral analysis was essentially performed as previously described (Xu et al., 2012).

SUPPLEMENTAL INFORMATION

Supplemental Information includes Supplemental Experimental Procedures and seven figures and can be found with this article online at http://dx.doi.org/10.1016/j.cell.2015.06.056.

AUTHOR CONTRIBUTIONS

G.R.A. designed, performed, and analyzed most experiments; J.A., C.F., A.X.Y., D.W., and S.-J.L. contributed to specific experiments; K.T. generated the conditional KO mice; J.C. contributed Ca^{2+} imaging tools; G.R.A., L.C., R.C.M., and T.C.S. designed experiments and analyzed data; and T.C.S. wrote the paper with input from all of the authors.

ACKNOWLEDGMENTS

We would like to thank Dr. Wei Xu and Dr. Theodoros Tsetsenis for advice on fear conditioning experiments and Dr. Ken Mackie (Indiana University) for his generous contribution of CB1R antibodies, which were used in this study. This paper was supported by grants from the NIH (R37 MH052804 to T.C.S.; K99 MH103531 to J.A.; K99 DA034029 to C.F.; P50 MH086403 to R.C.M., T.C.S., and L.C.) and from Autism Speaks (7953) (to G.R.A.).

Received: September 30, 2014
Revised: April 10, 2015
Accepted: June 8, 2015
Published: July 23, 2015

REFERENCES

Aoto, J., Martinelli, D.C., Malenka, R.C., Tabuchi, K., and Südhof, T.C. (2013). Presynaptic neurexin-3 alternative splicing trans-synaptically controls postsynaptic AMPA receptor trafficking. Cell *154*, 75–88.

Aoto, J., Földy, C., Ilcus, S.M., Tabuchi, K., and Südhof, T.C. (2015). Distinct circuit-dependent functions of presynaptic neurexin-3 at GABAergic and glutamatergic synapses. Nat. Neurosci. *18*, 997–1007.

Bang, M.L., and Owczarek, S. (2013). A matter of balance: role of neurexin and neuroligin at the synapse. Neurochem. Res. *38*, 1174–1189.

Behr, J., Wozny, C., Fidzinski, P., and Schmitz, D. (2009). Synaptic plasticity in the subiculum. Prog. Neurobiol. *89*, 334–342.

Boucard, A.A., Chubykin, A.A., Comoletti, D., Taylor, P., and Südhof, T.C. (2005). A splice code for trans-synaptic cell adhesion mediated by binding of neuroligin 1 to alpha- and beta-neurexins. Neuron *48*, 229–236.

Brown, S.P., Safo, P.K., and Regehr, W.G. (2004). Endocannabinoids inhibit transmission at granule cell to Purkinje cell synapses by modulating three types of presynaptic calcium channels. J. Neurosci. *24*, 5623–5631.

Castillo, P.E., Younts, T.J., Chávez, A.E., and Hashimotodani, Y. (2012). Endocannabinoid signaling and synaptic function. Neuron *76*, 70–81.

Chih, B., Gollan, L., and Scheiffele, P. (2006). Alternative splicing controls selective trans-synaptic interactions of the neuroligin-neurexin complex. Neuron *51*, 171–178.

Clarke, R.A., and Eapen, V. (2014). Balance within the neurexin trans-synaptic connexus stabilizes behavioral control. Front. Hum. Neurosci. *8*, 52.

Comoletti, D., Flynn, R.E., Boucard, A.A., Demeler, B., Schirf, V., Shi, J., Jennings, L.L., Newlin, H.R., Südhof, T.C., and Taylor, P. (2006). Gene selection, alternative splicing, and post-translational processing regulate neuroligin selectivity for β-neurexins. Biochemistry *45*, 12816–12827.

de Wit, J., Sylwestrak, E., O'Sullivan, M.L., Otto, S., Tiglio, K., Savas, J.N., Yates, J.R., 3rd, Comoletti, D., Taylor, P., and Ghosh, A. (2009). LRRTM2 interacts with Neurexin1 and regulates excitatory synapse formation. Neuron *64*, 799–806.

Di Marzo, V., Bifulco, M., and De Petrocellis, L. (2004). The endocannabinoid system and its therapeutic exploitation. Nat. Rev. Drug Discov. *3*, 771–784.

Fanselow, M.S., and Dong, H.W. (2010). Are the dorsal and ventral hippocampus functionally distinct structures? Neuron *65*, 7–19.

Földy, C., Malenka, R.C., and Südhof, T.C. (2013). Autism-associated neuroligin-3 mutations commonly disrupt tonic endocannabinoid signaling. Neuron *78*, 498–509.

Fowler, S.C., Birkestrand, B.R., Chen, R., Moss, S.J., Vorontsova, E., Wang, G., and Zarcone, T.J. (2001). A force-plate actometer for quantitating rodent behaviors: illustrative data on locomotion, rotation, spatial patterning, stereotypies, and tremor. J. Neurosci. Methods *107*, 107–124.

Freund, T.F., Katona, I., and Piomelli, D. (2003). Role of endogenous cannabinoids in synaptic signaling. Physiol. Rev. *83*, 1017–1066.

Graves, A.R., Moore, S.J., Bloss, E.B., Mensh, B.D., Kath, W.L., and Spruston, N. (2012). Hippocampal pyramidal neurons comprise two distinct cell types that are countermodulated by metabotropic receptors. Neuron *76*, 776–789.

Hajos, N., Ledent, C., and Freund, T.F. (2001). Novel cannabinoid-sensitive receptor mediates inhibition of glutamatergic synaptic transmission in the hippocampus. Neuroscience *106*, 1–4.

Han, J., Kesner, P., Metna-Laurent, M., Duan, T., Xu, L., Georges, F., Koehl, M., Abrous, D.N., Mendizabal-Zubiaga, J., Grandes, P., et al. (2012). Acute cannabinoids impair working memory through astroglial CB1 receptor modulation of hippocampal LTD. Cell *148*, 1039–1050.

Hessler, N.A., Shirke, A.M., and Malinow, R. (1993). The probability of transmitter release at a mammalian central synapse. Nature *366*, 569–572.

Ichtchenko, K., Hata, Y., Nguyen, T., Ullrich, B., Missler, M., Moomaw, C., and Südhof, T.C. (1995). Neuroligin 1: a splice site-specific ligand for beta-neurexins. Cell *81*, 435–443.

Kaeser, P.S., and Regehr, W.G. (2014). Molecular mechanisms for synchronous, asynchronous, and spontaneous neurotransmitter release. Annu. Rev. Physiol. *76*, 333–363.

Kaeser, P.S., Deng, L., Wang, Y., Dulubova, I., Liu, X., Rizo, J., and Südhof, T.C. (2011). RIM proteins tether Ca2+ channels to presynaptic active zones via a direct PDZ-domain interaction. Cell *144*, 282–295.

Kano, M., Ohno-Shosaku, T., Hashimotodani, Y., Uchigashima, M., and Watanabe, M. (2009). Endocannabinoid-mediated control of synaptic transmission. Physiol. Rev. *89*, 309–380.

(E) The model for β-neurexin action. In wild-type excitatory synapses (left), presynaptic β-neurexins regulate endocannabinoid signaling by controlling postsynaptic 2-AG synthesis, possibly via trans-synaptic interaction with postsynaptic neuroligin isoforms that exclusively bind to β-neurexins, but not α-neurexins, lacking an insert in SS#4. In excitatory β-neurexin KO synapses (right), 2-AG synthesis is disinhibited, CB1Rs are activated, and synaptic strength is decreased; moreover, in burst-firing subiculum neurons LTP is blocked, which may be responsible for the impairment in contextual memory.
See also Figure S7.

Katona, I., and Freund, T.F. (2008). Endocannabinoid signaling as a synaptic circuit breaker in neurological disease. Nat. Med. *14*, 923–930.

Katona, I., Urban, G.M., Wallace, M., Ledent, C., Jung, K.M., Piomelli, D., Mackie, K., and Freund, T.F. (2006). Molecular composition of the endocannabinoid system at glutamatergic synapses. J. Neurosci. *26*, 5628–5637.

Kawamura, Y., Fukaya, M., Maejima, T., Yoshida, T., Miura, E., Watanabe, M., Ohno-Shosaku, T., and Kano, M. (2006). The CB1 cannabinoid receptor is the major cannabinoid receptor at excitatory presynaptic sites in the hippocampus and cerebellum. J. Neurosci. *26*, 2991–3001.

Ko, J., Fuccillo, M.V., Malenka, R.C., and Südhof, T.C. (2009). LRRTM2 functions as a neurexin ligand in promoting excitatory synapse formation. Neuron *64*, 791–798.

Kreitzer, A.C., and Regehr, W.G. (2001). Retrograde inhibition of presynaptic calcium influx by endogenous cannabinoids at excitatory synapses onto Purkinje cells. Neuron *29*, 717–727.

Krueger, D.D., Tuffy, L.P., Papadopoulos, T., and Brose, N. (2012). The role of neurexins and neuroligins in the formation, maturation, and function of vertebrate synapses. Curr. Opin. Neurobiol. *22*, 412–422.

Matsuda, K., and Yuzaki, M. (2011). Cbln family proteins promote synapse formation by regulating distinct neurexin signaling pathways in various brain regions. Eur. J. Neurosci. *33*, 1447–1461.

Melis, M., Greco, B., and Tonini, R. (2014). Interplay between synaptic endocannabinoid signaling and metaplasticity in neuronal circuit function and dysfunction. Eur. J. Neurosci. *39*, 1189–1201.

Missler, M., Zhang, W., Rohlmann, A., Kattenstroth, G., Hammer, R.E., Gottmann, K., and Südhof, T.C. (2003). α-neurexins couple Ca^{2+} channels to synaptic vesicle exocytosis. Nature *423*, 939–948.

Murataeva, N., Straiker, A., and Mackie, K. (2014). Parsing the players: 2-arachidonoylglycerol synthesis and degradation in the CNS. Br. J. Pharmacol. *171*, 1379–1391.

Ohno-Shosaku, T., Tsubokawa, H., Mizushima, I., Yoneda, N., Zimmer, A., and Kano, M. (2002). Presynaptic cannabinoid sensitivity is a major determinant of depolarization-induced retrograde suppression at hippocampal synapses. J. Neurosci. *22*, 3864–3872.

Peterfi, Z., Urban, G.M., Papp, O.I., Nemeth, B., Monyer, H., Szabo, G., Erdelyi, F., Mackie, K., Freund, T.F., Hajos, N., et al. (2012). Endocannabinoid-mediated long-term depression of afferent excitatory synapses in hippocampal pyramidal cells and GABAergic interneurons. J. Neurosci. *32*, 14448–14463.

Petrenko, A.G., Ullrich, B., Missler, M., Krasnoperov, V., Rosahl, T.W., and Südhof, T.C. (1996). Structure and evolution of neurexophilin. J. Neurosci. *16*, 4360–4369.

Rosenmund, C., Clements, J.D., and Westbrook, G.L. (1993). Nonuniform probability of glutamate release at a hippocampal synapse. Science *262*, 754–757.

Rowen, L., Young, J., Birditt, B., Kaur, A., Madan, A., Philipps, D.L., Qin, S., Minx, P., Wilson, R.K., Hood, L., and Graveley, B.R. (2002). Analysis of the human neurexin genes: alternative splicing and the generation of protein diversity. Genomics *79*, 587–597.

Siddiqui, T.J., Pancaroglu, R., Kang, Y., Rooyakkers, A., and Craig, A.M. (2010). LRRTMs and neuroligins bind neurexins with a differential code to cooperate in glutamate synapse development. J. Neurosci. *30*, 7495–7506.

Staff, N.P., Jung, H.Y., Thiagarajan, T., Yao, M., and Spruston, N. (2000). Resting and active properties of pyramidal neurons in subiculum and CA1 of rat hippocampus. J. Neurophysiol. *84*, 2398–2408.

Südhof, T.C. (2008). Neuroligins and neurexins link synaptic function to cognitive disease. Nature *455*, 903–911.

Szabó, G.G., Lenkey, N., Holderith, N., Andrási, T., Nusser, Z., and Hájos, N. (2014). Presynaptic calcium channel inhibition underlies CB_1 cannabinoid receptor-mediated suppression of GABA release. J. Neurosci. *34*, 7958–7963.

Tabuchi, K., and Südhof, T.C. (2002). Structure and evolution of neurexin genes: insight into the mechanism of alternative splicing. Genomics *79*, 849–859.

Takahashi, K.A., and Castillo, P.E. (2006). The CB1 cannabinoid receptor mediates glutamatergic synaptic suppression in the hippocampus. Neuroscience *139*, 795–802.

Treutlein, B., Gokce, O., Quake, S.R., and Südhof, T.C. (2014). Cartography of neurexin alternative splicing mapped by single-molecule long-read mRNA sequencing. Proc. Natl. Acad. Sci. USA *111*, E1291–E1299.

Twitchell, W., Brown, S., and Mackie, K. (1997). Cannabinoids inhibit N- and P/Q-type calcium channels in cultured rat hippocampal neurons. J. Neurophysiol. *78*, 43–50.

Uemura, T., Lee, S.J., Yasumura, M., Takeuchi, T., Yoshida, T., Ra, M., Taguchi, R., Sakimura, K., and Mishina, M. (2010). Trans-synaptic interaction of GluRdelta2 and Neurexin through Cbln1 mediates synapse formation in the cerebellum. Cell *141*, 1068–1079.

Ullrich, B., Ushkaryov, Y.A., and Südhof, T.C. (1995). Cartography of neurexins: more than 1000 isoforms generated by alternative splicing and expressed in distinct subsets of neurons. Neuron *14*, 497–507.

Ushkaryov, Y.A., Petrenko, A.G., Geppert, M., and Südhof, T.C. (1992). Neurexins: synaptic cell surface proteins related to the alpha-latrotoxin receptor and laminin. Science *257*, 50–56.

Ushkaryov, Y.A., Hata, Y., Ichtchenko, K., Moomaw, C., Afendis, S., Slaughter, C.A., and Südhof, T.C. (1994). Conserved domain structure of beta-neurexins. Unusual cleaved signal sequences in receptor-like neuronal cell-surface proteins. J. Biol. Chem. *269*, 11987–11992.

van Welie, I., Remme, M.W., van Hooft, J.A., and Wadman, W.J. (2006). Different levels of Ih determine distinct temporal integration in bursting and regular-spiking neurons in rat subiculum. J. Physiol. *576*, 203–214.

Wozny, C., Maier, N., Fidzinski, P., Breustedt, J., Behr, J., and Schmitz, D. (2008). Differential cAMP signaling at hippocampal output synapses. J. Neurosci. *28*, 14358–14362.

Xu, J., Pang, Z.P., Shin, O.H., and Südhof, T.C. (2009). Synaptotagmin-1 functions as a Ca^{2+} sensor for spontaneous release. Nat. Neurosci. *12*, 759–766.

Xu, W., Morishita, W., Buckmaster, P.S., Pang, Z.P., Malenka, R.C., and Südhof, T.C. (2012). Distinct neuronal coding schemes in memory revealed by selective erasure of fast synchronous synaptic transmission. Neuron *73*, 990–1001.

Supplemental Figures

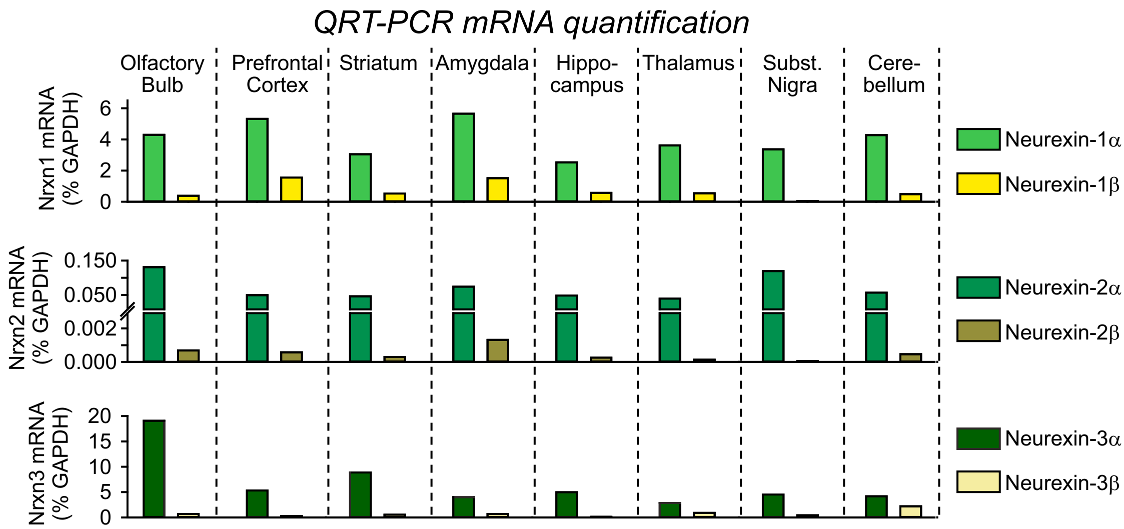

Figure S1. Expression Levels of α- and β-Neurexin mRNAs in Different Brain Regions Displayed as a Percentage of GAPDH Expression Levels, Related to Figure 1

mRNA levels were quantified in various brain regions of P30 mice using qRT-PCR. Data display the relative abundance of the α- and β-forms of the neurexin-1, -2, and -3 mRNAs normalized for those of glyceraldehyde-3-phosphate dehydrogenase (GAPDH) as an internal control (n = 3 mice).

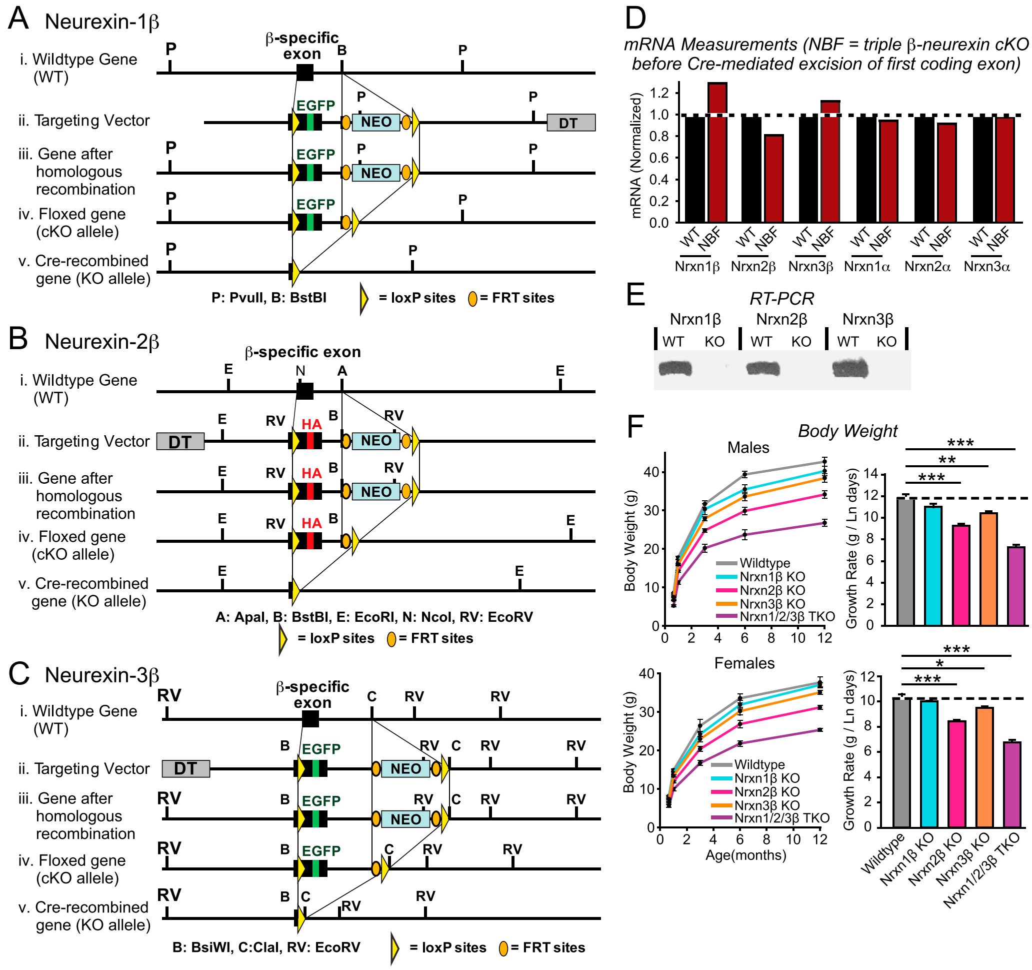

Figure S2. Gene Targeting Strategy for Generation of β-Neurexin-Specific cKO Mice, Evidence that the cKO Mice Express β-Neurexins Normally prior to Cre Recombination and that the KO Blocks β-Neurexin Expression, and Demonstration that the Constitutive β-Neurexin KO Causes Failure to Thrive as Revealed in a Reduced Body Weight, Related to Figure 1

(A–C) Schematic diagrams of the gene targeting strategies for neurexin-1β (A), -2β (B), and -3β (C). For all genes, a loxP site was introduced into the 5′ UTR in the β-neurexin-specific exon that encodes the N-terminal sequence of the respective β-neurexin, and an additional loxP site was introduced into the intron 3′ to this exon. In the neurexin-1β and neurexin-3β exons, an EGFP-coding sequence was introduced into the N-terminal sequence immediately after the signal peptide; in the neurexin-2β exon, an HA-epitope was inserted into the same position. In addition, a neomycin resistance gene cassette (NEO) flanked by Frt sites was introduced into the 3′ intron adjacent to the 3′ loxP site for positive selection of homologously recombined ES cell colonies, and a diphtheria toxin gene (DT) was added to the homologous sequence for negative selection. All diagrams depict from top to bottom (i) the WT gene structure, (ii) the targeting vector design, (iii) the mutant floxed gene after homologous recombination, (iv) the floxed cKO allele after excision of the neomycin resistance cassette by Frt recombinase; and (v) the KO allele after Cre-recombinase excision of the floxed exon. The targeting vectors were used to make mutant mice carrying the 'iii' allele, which was then converted into the cKO allele using Frt recombinase expressed in the germline. Mice were also converted into constitutive β-neurexin KO mice using Cre-recombinase expressed in the germline.

(D) Measurements of mRNA levels in whole brain (P30) from wild-type mice (WT) and β-neurexin triple cKO mice (NBF) using qRT-PCR. mRNA levels in NBF mice (standardized for GAPDH as an internal standard) were normalized to those of WT mice (n = 3 mice).

(E) RT-PCR analysis of β-neurexin triple KO mice confirms that the conditional exonic deletion completely ablates β-neurexin gene expression. The 5′ primers used target the unique β-neurexin specific exons not shared with their α-neurexin counterparts. The 3′ primers target the downstream adjacent exons that are shared between both α- and β-neurexin. Shown reaction products have the predicted molecular weight expected after removal of the genomic intron between these two targeted exons.

(F) Body weight measurements of littermate single constitutive β-neurexin KO mice and of non-littermate triple β-neurexin KO (TKO) mice over the course of a full year (n = 3 mice for each cohort of males (*top*) and females (*bottom*); *left*, growth curves; *right*, growth rates as determined by fitting a linear regression curve to the relation of body weight as a function of age (taking the natural logarithm of age = Ln days)). Note the dramatic reduction in weight not only of the triple β-neurexin KO mice, but also of the single neurexin-2β and −3β KO mice despite the relatively low expression levels of neurexin-2β compared to those of neurexin-1β or −3β (Figures 1A and S1). Data shown are means ± SEM. Statistical comparisons of the left plots using one-way ANOVA of the KO conditions to the WT revealed $p < 0.01$ for the Nrxn2β KO condition and $p < 0.001$ for the triple KO at all time points. For the summary graphs, statistical analysis was performed by Student's t test (*$p < 0.05$, **$p < 0.01$, ***$p < 0.001$).

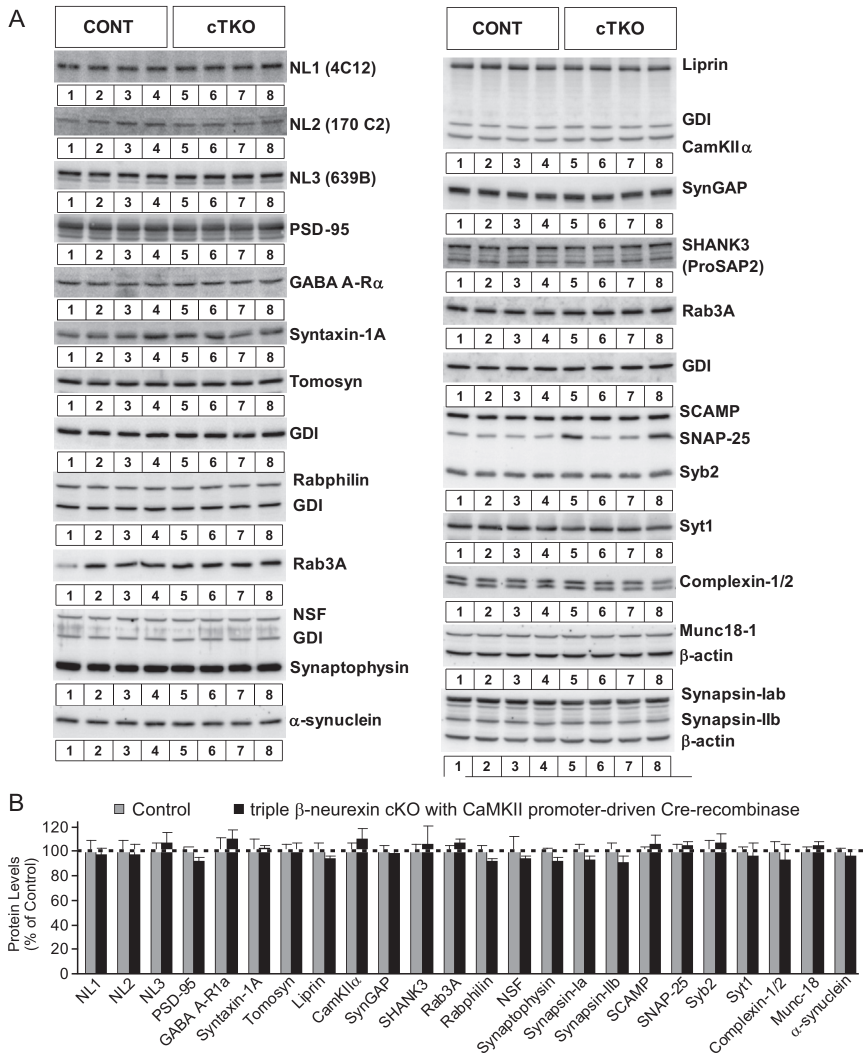

Figure S3. Synaptic Protein Composition in Mice with a Deletion of β-Neurexins in Excitatory Forebrain Neurons Using Transgenic Cre-Expression Driven by the CaMKII Promoter, Related to Figure 1

(A and B) Triple β-neurexin cKO mice were crossed with transgenic mice expressing Cre-recombinase under control of the CaMKIIα promoter (Jackson Laboratory Strain Name B6.Cg-Tg(CamK2a-cre)T29-1Stl/J) to produce normally developed mice with broad deletion of β-neurexins in forebrain neurons. Although these conditions delete β-neurexins only in excitatory neurons, this approach was necessary because the failure to thrive of the constitutive germline triple KO mice would otherwise introduce a confounding influence on protein levels (see Figure S2). However, no other experiments in this paper use these transgenic Cre-mice to delete β-neurexins because viral manipulations are superior to the transgenic CaMKII-Cre approach in order to achieve temporally and spatially defined deletions of β-neurexins and in order to also target inhibitory neurons. (A) Representative immunoblots of forebrain homogenates prepared from adult wild-type (Control) and homozygous β-neurexin triple cKO mice (cTKO) with Cre-expression driven by the CaMKIIα promoter. Mice were analyzed at P30. (B) Measurements of protein levels in brain homogenates from control and cTKO mice using quantitative immunoblotting with ^{125}I-labeled secondary antibodies and phosphoimager detection. Data shown are means ± SEM (n = 4) from three independent determinations normalized for signals obtained with antibodies to GDP dissociating inhibitor (GDI) and β-actin as internal standards.

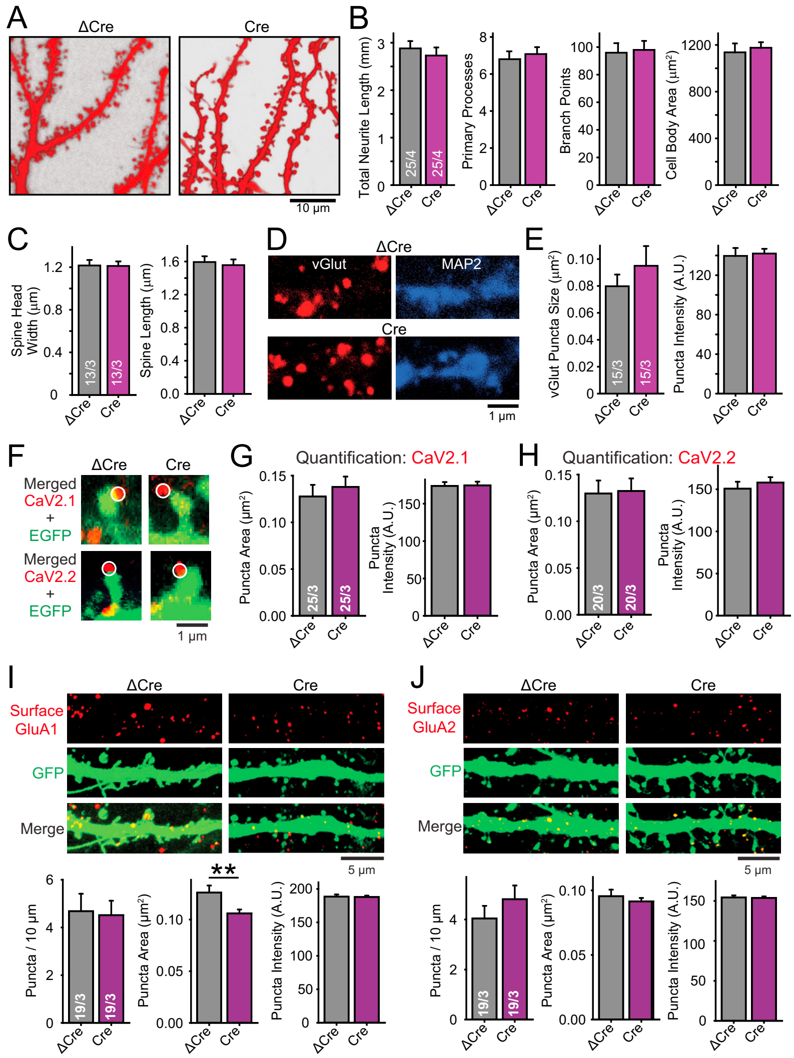

Figure S4. Conditional KO of β-Neurexins in Cultured Cortical Neurons Does Not Alter Neuronal Morphology or Localization and Levels of Presynaptic Ca^{2+} Channels but Produces a Small Decrease in Postsynaptic AMPARs, Related to Figures 1, 2, and 3

(A) Images of representative spiny dendritic branches of cortical pyramidal neurons from β-neurexin triple cKO neurons infected with lentiviruses that express ΔCre (left) and Cre (right). Neurons were filled with Alexa Fluor 594 via a patch pipet for imaging.

(B and C) Quantitative morphological properties of Alexa-dye filled neurons as described in (A). Shown are quantifications of total dendritic length (B, left), primary processes originating from the soma (B, left middle), dendrite branching points (B, right middle), soma size (B, right), spine head width (C, left), and protrusion length from the dendritic shaft (C, right).

(D and E) Representative images of neurons stained for the presynaptic excitatory marker vGlut1 and the dendritic marker MAP2 (D), and summary graphs of vGlut1 puncta size and staining intensity (E). Data complement data of Figure 1E.

(F–H) Conditional KO of β-neurexins in cultured cortical neurons does not alter presynaptic voltage-gated Ca^{2+}-channel levels and localization at spine synapses. Cortical neurons cultured from β-neurexin triple cKO mice were infected with lentiviruses expressing either inactive (ΔCre) or active cre-recombinase (Cre), and sparsely transfected with an EGFP expression vector for visualization of neuronal morphology. Cells were analyzed by immunolabeling for presynaptic voltage-gated P/Q-type (CaV2.1) and N-type (CaV2.2) Ca^{2+}-channels as indicated (F, same images as in Figure 2F but with the ROIs circled; G and H, summary graphs of the Ca^{2+}-channel immunoreactivity puncta size and staining intensity, quantified for puncta that associate with postsynaptic pyramidal neuron spine structures). Data extend the analysis of Figure 2F.

(I and J) Conditional KO of β-neurexins in cultured cortical neurons causes a small reduction in the surface level of GluA1 AMPARs consistent with the small decrease in mEPSC amplitude (Figure 3) and with the effect of neurexin-3 manipulations in hippocampal neurons (Aoto et al., 2013). Neurons obtained as described for F-H were analyzed by surface-labeling for GluA1 (I) or GluA2 AMPARs (J). For each set of panels, representative images of cortical pyramidal neurons identified by EGFP expression are shown on the top, and summary graphs of morphological parameters on the bottom (left, puncta density along secondary/tertiary dendrites; center, puncta size; right, staining intensity).

Data shown are means ± SEM; numbers of neurons/independent cultures examined are shown in the graphs. Statistical analysis was performed by Student's t test (**$p < 0.01$).

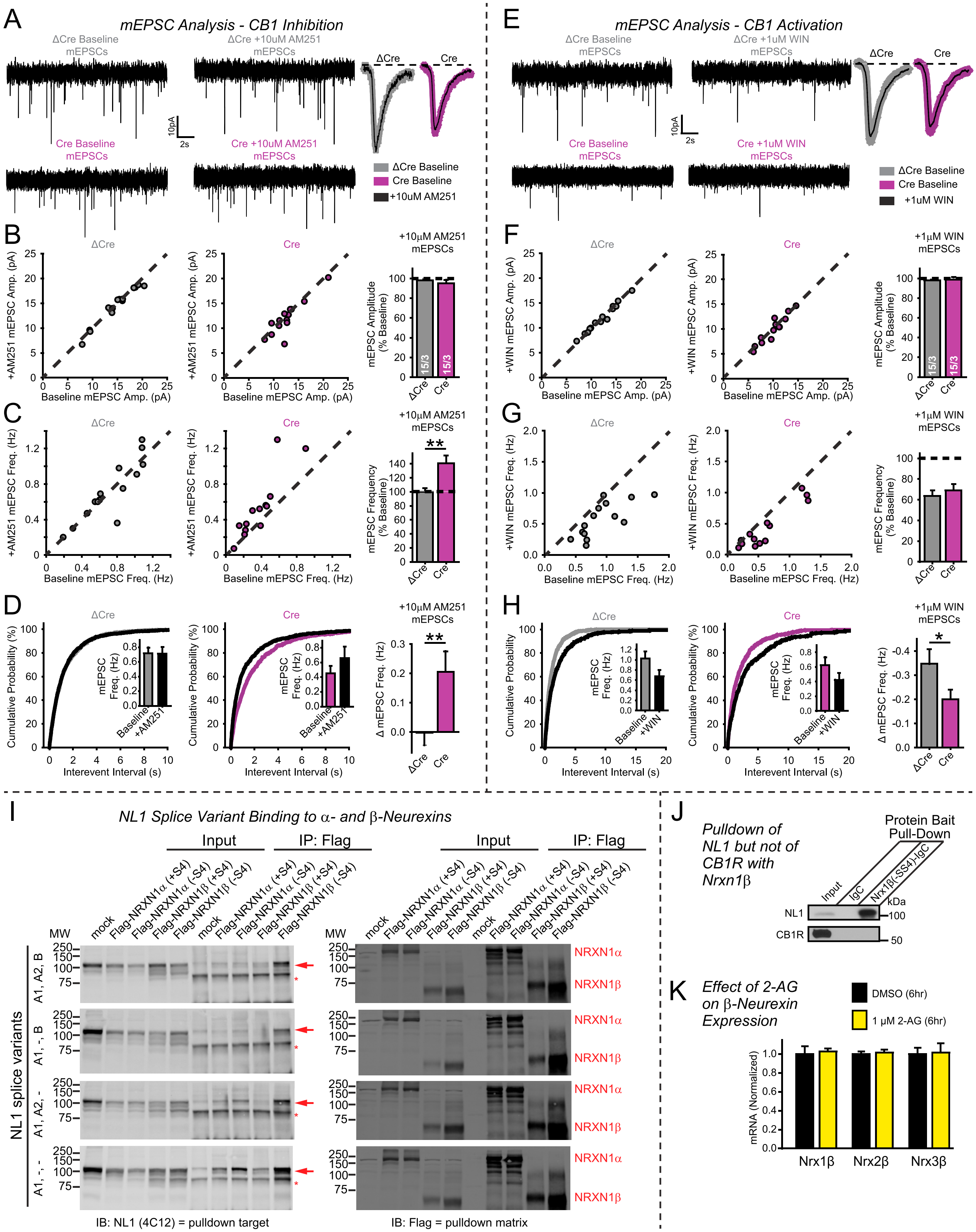

(legend on next page)

Figure S5. Conditional KO of β-Neurexins Enhances Basal Endocannabinoid Signaling at Excitatory Synapses; Some Neuroligin-1 Splice Variants Selectively Bind Only to Neurexin-1β, but Not to Neurexin-1α; Neurexin-1β Is Able to Pull Down Neuroligin-1, but Not CB1 Receptors; and Addition of the Endocannabinoid 2-AG Does Not Alter β-Neurexin Expression, Related to Figures 3 and 4

(A) (Left) Using cultured cortical neurons infected with ΔCre (top) and Cre (bottom) expressing lentiviruses, we recorded 2 min baselines of miniature excitatory post-synaptic currents (mEPSCs) and (middle) another 2-min window of mEPSCs 5 min after the application of 10 μM AM251. Shown are representative recording traces. (Right) Shown are averaged individual events for both ΔCre and Cre infected neurons during baseline and after AM251 application.

(B and C) Single neuron mEPSC averaged amplitudes (B), and frequencies (C), shown for baseline (x axis) and after exposure to AM251 (y axis). Linear relationships are shown with dashed line. Shown are mEPSC recordings from ΔCre (left), Cre (middle), and summary graphs (right).

(D) Frequency of event cumulative distributions and cell averages (inset) for analyzed mEPSCs during baseline and after AM251 addition for ΔCre (left) and Cre (middle). *Right*, summary graphs of change in event frequencies after AM251 addition.

(E–H) Same as in (A)–(D), except that recordings were made 5 min after application of 1 μM WIN 55,212-2 mesylate (WIN).

(I) Demonstration that some splice variants of NL1 specifically bind only to neurexin-1β but not neurexin-1α. Data are from co-immunoprecipitation experiments of different NL1 splice variants with neurexin-1α or neurexin-1β containing or lacking an insert in SS#4. Proteins were solubilized from HEK cells co-transfected with expression plasmids for Flag-tagged neurexin-1α or −1β as indicated and for four different NL1 splicing variants containing or lacking inserts in splice sites A1, A2, and B (terminology after Comoletti et al., 2006). Neurexin-1 was immunoprecipitated with Flag antibodies, and input fractions and immunoprecipitates were immunoblotted for NL1 *(left)* and for Flag-tagged neurexin-1 *(right)*. Arrows indicate NL1, and asterisks non-specific signals.

(J) Lack of direct interaction between neurexin-1β lacking an insert in SS#4 (which rescue the β-neurexin KO phenotype) and CB1-receptors. Solubilized proteins from total mouse brain homogenates (input) were applied to protein-A Sepharose beads containing 5 μg immobilized Ig control protein (IgC), or neurexin-1β Ig-fusion protein (N1β(-SS4)-IgC). Beads were washed three times with solubilization buffer and bound proteins were eluted with SDS sample buffer. Proteins were analyzed by SDS-PAGE and immunoblotting with NL1 antibodies (4C12) as a positive control for neurexin1β(-SS4) binding, as well as CB1R antibody (CT).

(K) β-Neurexin mRNA is unaltered by stimulation of neurons with the CB1-receptor agonist 2-AG. mRNA levels were quantified in cultured wild-type cortical neurons treated for 6 hr with either DMSO or 1 μM 2-AG endocannabinoid using qRT-PCR. Summary graph displays the relative abundance of neurexin-1β, -2β, and -3β mRNAs normalized to DMSO control average (n = 4 treatments /two independent cultures).

Data shown are means ± SEM; numbers of neurons/independent cultures examined are shown in the graphs for A-H. Statistical analysis was performed by Student's t test (*p < 0.05, **p < 0.01).

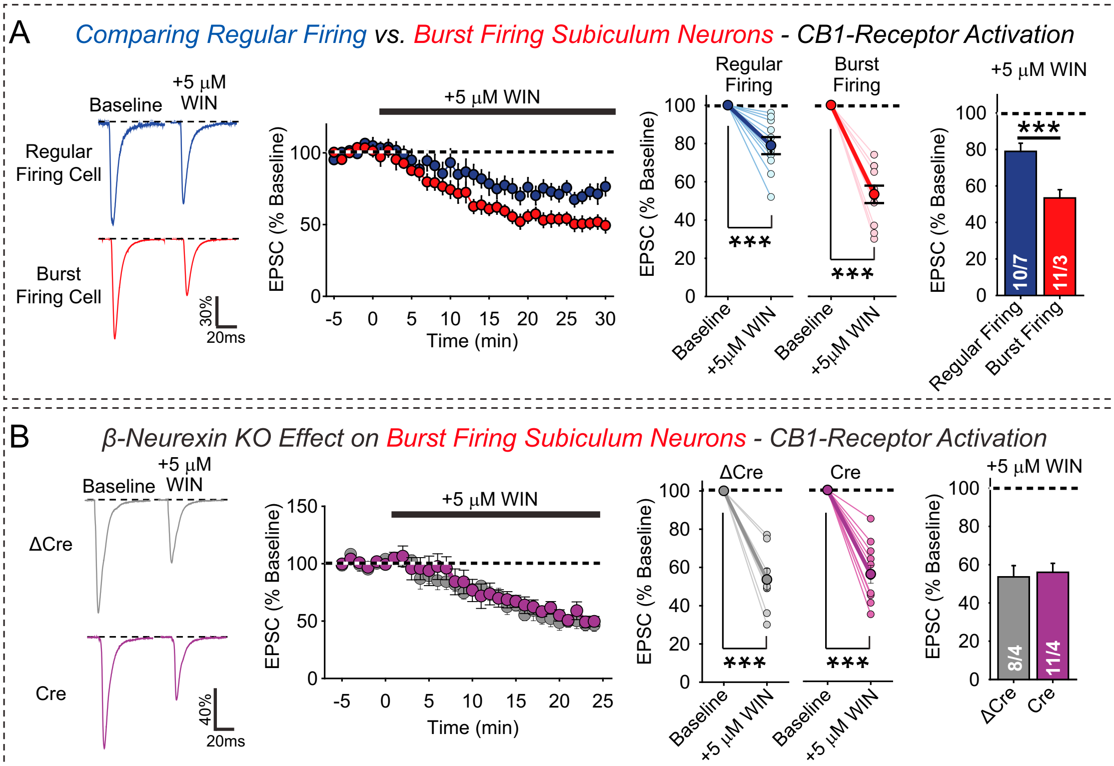

Figure S6. Synapses Formed by Presynaptic CA1-Region Neurons onto Postsynaptic Regular-Firing and Burst-Firing Subiculum Neurons Are Differentially Controlled by CB1-Receptor Signaling, but the CB1-Receptor Agonist WIN Has Similar Relative Effects on Control and β-Neurexin KO Neurons in Burst-Firing Neurons, Related to Figure 5

(A) Assessment of endocannabinoid signaling in regular-firing and burst-firing subiculum neurons in wild-type mice using a CB1R agonist WIN55,212-2 mesylate (WIN). EPSCs were elicited in acute slices by stimulation of CA1 axons at 0.1 Hz, and analyzed by whole-cell recordings. After establishing a baseline for ~5 min, the CB1R agonist WIN was bath applied, and EPSCs were monitored for 20-30 min (*left*, representative EPSC traces; *left middle*, plots of the relative EPSC amplitude as a function of time; *right middle*, plots of the relative WIN-induced changes in individual neurons; *right*, summary graphs of the mean WIN-induced amplitude changes.

(B) Effect of presynaptic β-neurexin KO on CB1R-mediated synapse modulation in synapses formed by CA1-region pyramidal neurons onto burst firing subiculum neurons. The experiments were performed essentially as described for (A), except that only burst firing neurons were analyzed, and that slices were obtained from triple β-neurexin cKO mice that had been stereotactically injected in the CA1 region with AAVs expressing ΔCre- or Cre-EGFP fusion proteins. Note that although by other measures, β-neurexin KO samples differ from control samples in terms of endocannabinoid signaling, they are indistinguishable in this experiment probably because the data are analyzed in relative terms to decrease the number of experiments required. Since the β-neurexin KO neurons start off with a lower synaptic strength than control neurons, differences in the further depression of synaptic strength by WIN may be difficult to detect in this experimental configuration.

Data shown are means ± SEM; numbers of neurons/mice examined are shown in the summary graphs. Statistical analysis was performed by paired Student's t test for WIN effect in single cell plots, and unpaired Student's t test for comparisons in right summary graphs (***$p < 0.001$).

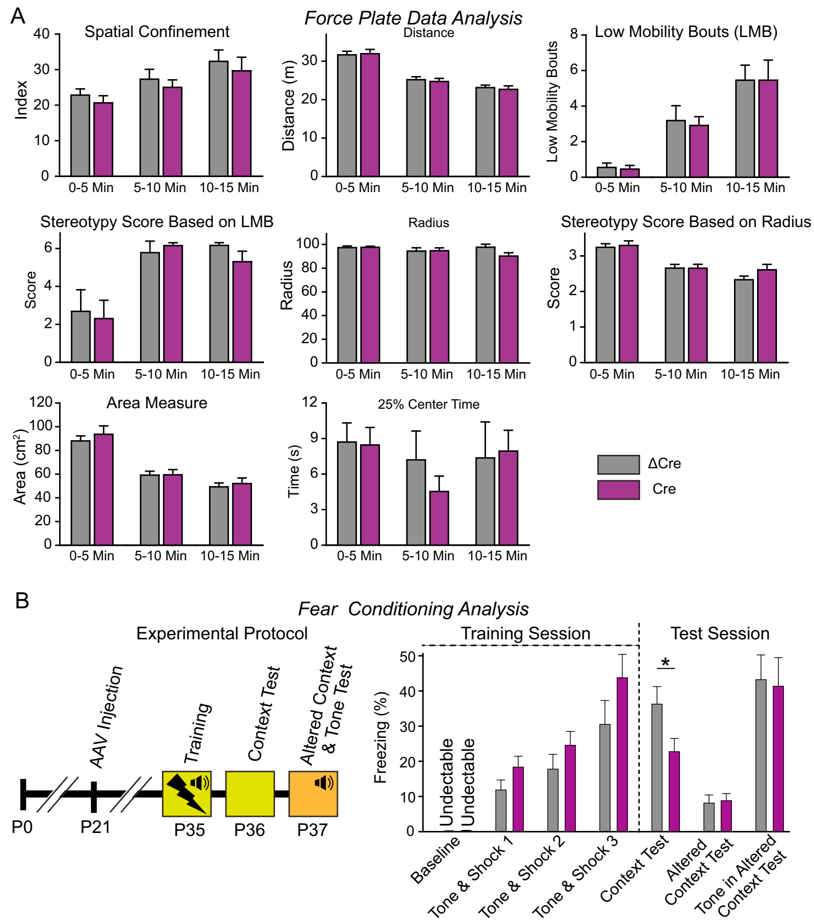

Figure S7. Open-Field Analysis and Fear Conditioning of β-Neurexin cKO Mice Injected with ΔCre- and Cre-Expressing AAVs Targeting Hippocampal CA1, Related to Figure 7

(A) Force-plate actometer analysis of β-neurexin cKO Injected with ΔCre and Cre expressing AAVs targeting hippocampal CA1. β-neurexin cKO mice stereotactically injected with ΔCre and Cre expressing AAVs targeting hippocampal CA1 (Figure 7) were analyzed by the same standard force-plate actometer procedure as described previously (Fowler et al., 2001). Analyses were performed before memory tests had been performed, and initiated by placing mice individually into the center of a force-plate actometer (28 × 28 cm). The actometer accurately monitors all mouse movements, allowing a precise quantitation of various types of movements over the observation period (15 min total, divided into three 5 min segments). The spatial confinement score reflects the deviation of the set of position coordinates in a session from the uniform distribution of the 64 separate 3.5 × 3.5 cm squares covering the entire force plate surface. The maximum score 99.216 indicated that a mouse (the center of force) stayed in one square for the entire session while the minimum score 0 indicated that a mouse equally visited each square. The distance was the total distance traveled in the session, which was the line integral of movement of the center of force. Low mobility bouts were defined as bouts during which the center of force remained inside a circle of 15-mm radius for more than 10 s. The stereotypy score based on low mobility bouts (LMB) was calculated as the movement of the center of force during low mobility bouts, expressed as distance per low mobility bout. Area measure was calculated as sum of triangle areas formed by three successive locations of the center of force in the session. The radius was another indicator of the spatial confinement, calculated as radius of the area of the points in this session. The stereotypy score (radius) was calculated as the distance divided by the radius measure per session. 25% center time was defined as the time in which the center of force (i.e., the mouse) remained inside the central square that occupies 25% of the actometer area. Data are means ± SEMs (n = 11).

(B) Loss of β-neurexins in the CA1-region hippocampus impairs fear contextual memory without interfering with fear-learning. *Left,* timeline of fear conditioning experiment. AAV injected β-neurexin cKO animals from above were tested for fear conditioned responses 2 weeks after injection, and after open field actometer analysis. Fear conditioning training was conducted by pairing 30 s auditory tones ending with 2 s footshocks, performed 3 times separated by 1 min intervals. Training context test was performed 24 hr after training to measure contextual memory. After another 24 hr, an altered-context test (similar cage but changes in odor, cage floor, wall patterning) was performed to test the precision of memory. Lastly, a 60 s tone test was delivered at the end of the altered context test in order to measure memory of auditory cues. *Right,* summary graph of fear conditioning experiments. Fear responses were monitored by measuring percent of time spent "freezing," defined as motionless bouts greater than 1 s. For training, mice were placed inside the conditioning chamber for 2 min (baseline – undectable freezing %), followed by 3 tone/footshock pairs (freezing measured during 1 min interval after tone/footshock). At 24 hr after training, animals were re-exposed to the conditioning chamber and measured freezing for 5 min (Context Test), to measure contextual memory. After another 24hrs, an altered-context test (similar cage but changes in odor, cage floor, wall patterning) was performed for 5 min to test the precision of memory. Lastly, a 60 s tone test was delivered at the end of the altered context test in order to measure memory of auditory cues. Data shown are means ± SEM; n = 11 mice. Statistical analysis was performed by Student's t test (*p < 0.05).

Cell

Supplemental Information

β-Neurexins Control Neural Circuits by Regulating Synaptic Endocannabinoid Signaling

Garret R. Anderson, Jason Aoto, Katsuhiko Tabuchi, Csaba Földy, Jason Covy, Ada Xin Yee, Dick Wu, Sung-Jin Lee, Lu Chen, Robert C. Malenka, and Thomas C. Südhof

Supplemental Experimental Procedures

Generation of Mutant Mice

Neurexin-β-floxed (NBF) mutant mice were generated by homologous recombination in R1 embryonic stem cells (Tabuchi et al., 2007) using the strategy outlined in Figure 1B / Supplemental Figure2 that targets the specific exon for each β-neurexin gene: Nrx1β – exon 18, Nrx2β – exon 17, Nrx3β – exon 17 (Tabuchi and Südhof, 2002). Each of the three targeted genes were modified by the insertion of a loxP site in the 5' UTR, and an Frt-flanked neomycin cassette with a 3' loxP site in the first intron of β-neurexins. The β-neurexin 1 and β-neurexin 3 genes received an additional green fluorescent protein (GFP) insertion in their unique first exon. The β-neurexin 2 gene was further modified with a hemagglutinin (HA) protein epitope insertion in its unique first exon. The genes were independently targeted in (129X1/SvJ x 129S1/Sv)F1- *Kitl*$^{+}$-derived R1 embryonic stem (ES) cells. Following homologous recombination, positive clones were validated by Southern blotting and PCR genotyping, and were injected into C57BL/6 blastocysts. Resultant germline mutant mice were crossed with a transgenic flipase (FLP) strain on a mixed C57BL/6 and 129 background to remove the neomycin resistance cassettes. The three mutations were intercrossed and backcrossed for more than 3 generations to C57BL/6 mice to generate homozygous triple conditional β-neurexin KO mice. Genotyping was performed using the following primers: Nrx1β – AAAGTTTGGGGCACAAGAAG / TGGGGTACTGTTGTAGGGCAC; Nrx2β – CGCTGCGCGTACCCCGGATTC / CCGGGGGCGGCCACCTTACAG; Nrx3β – GAAGAACTCCACACAGAGCTG / AAACCGATTCACCATTTCCCC. Conditional β-neurexin KO mice were also crossed to transgenic mice expressing Cre-recombinase to produce constitutive β-neurexin single, double, and triple KO mice for analysis (Fig. S2). Finally, conditional β-neurexin KO mice were crossed with transgenic mice expressing Cre-recombinase under control of the CaMKIIα promoter (Jackson Laboratory Strain Name B6.Cg-Tg(CamK2a-cre)T29-1Stl/J) to produce triple β-neurexin KO mice with broad deletion of β-neurexins in forebrain neurons but with normal overall development and normal body weights (see Fig. S3). All mouse work was performed as prescribed by approved protocols at Stanford University, and this mouse line was submitted to Jackson Labs (Stock Number: 008416) and is available for distribution.

Measurements of α- and β-Neurexin mRNA Levels in Mouse Brain

qRT-PCR on brain tissues was performed on RNA isolated from ~P30 mice using the RNAqueous-Micro RNA isolation kit (Invitrogen). 80 ng of total RNA was added to each reaction using the LightCycler 480 reagent kit (Roche). Reactions were run and analyzed using a 7900HT Fast RT-PCR instrument (Applied Biosystems) with GAPDH as an internal control. Real time QRT-PCR assays were either custom designed through Integrated DNA Technologies PrimeTime assays (Nrx1β primers AAGCATCATTCAGTGCCTATTG / GGCCACTTATATGTAATCTGTC and probe CTACAGGTCACCAGCATCCTTGCGAG;

Nrx2β primers CACTTCCACAGCAAGCAC / CTTCCCGAAGATGTATGTG and probe CGTGCCCATCGCCATCAACCGCA); Or predesigned by Life Technologies TaqMan Gene Expression Assays (Nrx3β - Mm01338630_m1; Nrx1α - Mm00660298_m1; Nrx2α - Mm01236864_g1; Nrx3α - Mm01335648_m1).

Neuronal Cultures

Cortical neurons were cultured from NBF mice as described (Maximov et al., 2007). Briefly, primary cortical neurons were isolated from P0-1 CD1 mice, dissociated by papain digestion, and plated on Matrigel (BD Biosciences)-coated glass coverslips. The neurons were cultured for 14-18 days *in vitro* in MEM (Gibco) supplemented with B27 (Gibco), glucose, transferrin, fetal bovine serum, and Ara-C.

Lentiviral Production and Infection of Cultured Neurons

Nuclear localized EGFP-Cre and EGFP-ΔCre fusion proteins deliverable by lentiviruses were from previously described vectors (Kaeser et al., 2011). All neurexin-1β rescue constructs were previously described mouse cDNAs expressed from separate lentiviruses (Aoto et al., 2013). The production of lentiviruses and infection of neurons with lentiviruses have been described (Pang et al., 2010). Briefly, the lentiviral expression vector and three helper plasmids (pRSV-REV, pMDLg/pRRE and vesicular stomatitis virus G protein (VSVG)) were co-transfected into human embryonic kidney (HEK) 293T cells (ATCC), at 6, 2, 2 and 2 µg of DNA per 25 cm2 culture area, respectively. Transfections were performed using calcium-phosphate method. Supernatant with viruses was collected 48 hours after transfection, spun at 500g for 5min to pellet cellular debris, and added to culture neurons. Cortical neuronal cultures were infected at DIV3-4 (3-4 days *in vitro*) and used for physiological analysis at DIV14-16.

AAV Preparation

For *in vivo* infections, we employed the AAV-DJ strain that is highly efficient *in vivo* (Xu et al., 2012). AAV vectors were constructed from an empty cloning vector where the expression cassette is as follows: left-ITR of AAV2, CMV promoter and beta-globin intron, multiple cloning site (MCS), hGH poly A sequence and right ITR. EGFP, inactive (ΔCre) and active (Cre) Cre-recombinase were inserted into the multiple cloning sites. AAV plasmids were co-transfected with pHelper and pRC-DJ into HEK293T cells. 72 hr post transfection, cells were harvested, lysed and run on an iodixanol gradient by ultracentrifugation at 100,000 g for 2 hr. The 40% iodixanol fraction containing AAV was collected, concentrated and washed in a 100K MWCO ultracon filter. The infectious titer of virus was measured by infecting HEK293 cells with serial dilutions, and used for stereotaxic infections at 1×10^7 infectious units/µl. NBF mutant mice in an SV129/Bl6 hybrid background were anesthetized with tribromoethanol (125-200 mg/kg) at P21-P23. AAV was injected with a glass pipette bilaterally into the CA1 region of the intermediate hippocampus (Bregma coordinates: AP: −3.2 mm, ML: ± 3.45 mm, DV: −2.7 mm; flow rate = 0.15 µl/min; injected volume = 0.85 µl). Efficiency and localization of AAV expression was confirmed by nuclear EGFP expression of inactive and active EGFP - Cre recombinase fusion protein expression by histochemistry.

Electrophysiology

Neuronal culture electrophysiological recordings were performed essentially as described (Maximov et al., 2007). Briefly, evoked synaptic responses were triggered with a 1-ms current injection (90 µA) by a nichrome wire electrode placed at a position 100-150 µm from the soma of neurons recorded. The patch pipettes were pulled from borosilicate glass capillary tubes (World Precision Instruments, Cat# TW150-4) using a PC-10 pipette puller (Narishige). The resistance of pipettes filled with intracellular solution varied between 3-5 MOhm. Synaptic currents were monitored with a Multiclamp 700B amplifier (Molecular Devices). The frequency, duration, and magnitude of the extracellular stimulus were controlled with a Model 2100 Isolated Pulse Stimulator (A-M Systems, Inc.) synchronized with Clampex 9 data acquisition software (Molecular Devices). For excitatory voltage-clamp recordings (AMPA-EPSCs, NMDA-EPSCs, mEPSC), a whole-cell pipette solution was used containing (in mM) 135 Cs-Methane-sulfonate, 15 CsCl, 8 NaCl, 10 Tetraethylammonium-Cl, 10 HEPES, 0.2 EGTA, 0.3 Na-GTP, 4 Na-ATP, and 10 QX-314 (pH 7.4, adjusted with CsOH). For inhibitory voltage-clamp recordings (GABA-IPSCs, mIPSC), a whole-cell pipette solution was used containing (in mM) 135 CsCl, 5 NaCl, 10 HEPES, 1 EGTA, 1 Na-GTP, 4 Mg-ATP and 10 QX-314 (pH 7.4, adjusted with CsOH). The bath solution of artificial cerebral spinal fluid (ACSF) contained (in mM) 140 NaCl, 5 KCl, 2 $CaCl_2$, 1.3 $MgCl_2$, 10 HEPES, 10 glucose (pH 7.4, adjusted with NaOH). Postsynaptic currents were pharmacologically isolated by adding the AMPA receptor blocker CNQX (20 µM), and/or NMDA receptor blocker AP-5 (50 µM), and/or the $GABA_A$ receptor blocker picrotoxin (50 µM) to the extracellular bath solution. AMPA-EPSCs and GABA-IPSCs were performed while holding the cell at -70mV, and NMDA-EPSCs at +40 mV. Spontaneous miniature postsynaptic currents (mIPSCs and mEPSCs) were monitored in the presence of tetrodotoxin (500 nM) to block action potentials, at -70mV holding potential. Synaptic currents were sampled at 10 kHz and analyzed offline using Clampfit 9 (Molecular Devices) software. For graphic representation, the stimulus artifacts of the current traces were removed. Miniature events were analyzed using the template matching search and a minimal threshold of 5 pA and each event was visually inspected for inclusion or rejection by an experimenter blind to the recording condition.

For acute slice electrophysiology performed on hippocampal subiculum neurons, AAV injected mice were used 2-3 weeks after infection. Horizontal hippocampal slices (300 µm) were cut in ice-cold solution containing (in mM): 85 NaCl, 75 Sucrose, 2.5 KCl, 1.3 NaH_2PO_4, 24 $NaHCO_3$, 0.5 $CaCl_2$, 4 $MgCl_2$, 25 D-Glucose saturated with 95% O_2/5% CO_2. Slices were transferred to a holding chamber containing artificial cerebrospinal fluid (ACSF, in mM): 126 NaCl, 2.5 KCl, 1 NaH_2PO_4, 26.2 $NaHCO_3$, 2.5 $CaCl_2$, 1.3 $MgSO_4$-

$7H_2O$, 11 D-Glucose, ~290 mOsm. Slices were allowed to recover at 31.5°C for 30 min then at room temp for 1 hr. Acute slices where transferred to a recording chamber continuously superfused with oxygenated ACSF (1.5 ml/min) maintained at 30.5°C. For whole-cell input/output, PPR and LTP experiments, 50 µM picrotoxin was added. A whole-cell pipette solution was used containing (in mM): 137 K-gluconate, 5 KCl, 10 HEPES, 4 ATP-Mg_2, 0.5 GTP-Na_2, 10 Phosphocreatine, 0.2 EGTA, pH 7.2 with KOH. Prior to recording EPSCs, upon establishing a whole-cell recording configuration, the recording pipet was switched to current clamp at resting membrane potential and depolarizing current steps in increments of +50pA were applied to characterize the cell's action potential firing behavior. After identification of the subiculum cell type, neurons were then voltage clamped at −70 mV for recording extracellular-evoked EPSCs. EPSCs were evoked by electrical stimulation with a nichrome electrode positioned on axonal fibers at the alveus – stratum oriens border above the distal region of the CA1. Paired-pulse values were collected at inter-stimulus intervals ranging from 40 ms to 400 ms. LTP in the subiculum was analyzed as previously described (Wozny et al., 2008). Briefly, four tetani of high-frequency stimulation were applied in current-clamp mode at resting membrane potential at 100 Hz for 1 s with 10 s intertrain intervals. Baseline and post-LTP induction EPSCs were sampled at 0.1 Hz and binned into 1 min epochs. The magnitude of LTP was assessed by averaging the last 10 min of each experiment (50-60 min after induction), in relation to the 10 min baseline recording period.

GCaMP5G-Syb2 Ca^{2+}-Imaging

Chimeric GCaMP5G-Syb2 was made using PCR primers tagged with restriction digestion linkers. GCaMP5G PCR was performed targeting full-length GCaMP5G using pCMV-GCaMP5G as template (Addgene; Plasmid 31788), with 5' primer tagged with BamH1 linker (ggatcccaccatgggttctcatcatcat) and 3' primer tagged with AgeI linker (accggtcttcgctgtcatcatttgtac). Synaptobrevin-2 PCR was performed targeting the full-length Synpatobrevin-2 after the initial methionine codon using pCMV5-Sbr2 (Burre et al., 2010) as template, with the 5' primer tagged with AgeI linker (accggttcggctaccgctgccaccgt) and 3' primer tagged with EcoRI linker (gaattcttaagtgctgaagtaaacg). Syb2 was direct cloned into lentiviral vector FSW (with synapsin promoter) using AgeI-EcoRI restriction sites to produce Syb2-FSW vector. GCaMP5G was subsequently added by restriction digestion cloning using BamHI-AgeI to produce GCaMP5G-Syb2-FSW vector.

To visualize neuronal morphology during imaging experiments, neurons were sparsely labeled by transfection of L309c mCherry expressing construct (Anderson et al., 2012). Imaging was performed on a Zeiss LSM 510 confocal microscope. GCaMP5G-Syb2 fluorescence was measured by excitation with a 488 nm laser (1% power), and collecting emission passed through a 500-530 nm band pass filter. Neuron morphology was visualized simultaneously by monitoring mCherry fluorescence by excitation with a 543 nm laser (10% power), and collecting emission passed through a 560 nm long pass filter. Pinhole was adjusted to 1 A.U.

To select for presynaptic analysis of calcium transients at excitatory synapses, regions of interest were defined by manual selection of GCaMP5G-Syb2 fluorescent presynaptic boutons that oppose postsynaptic spine heads marked by mCherry expression. GCaMP5G-Syb2 fluorescence was monitored with images acquired at a rate of 10 Hz. GCaMP5G-Syb2 fluorescent transients were elicited by nichrome wire electrode placed at a position 100-150 μm from the soma of neuron being recorded. Stimulus trains were applied at 1, 5, 10, 50, 100 stimuli at a rate of 50 Hz. To normalize amplitudes of fluorescence transients from within individual GCaMP5G-Syb2 boutons, responses were quantified as a fraction of the maximal fluorescence achieved in saturating Ca^{2+} concentrations defined as 100 stimuli at 50 Hz train. Fluorescent signals were quantified as mean region of interest and expressed as % $\Delta F_{sat} = 100*(F-F_0)/(F_{sat}-F_0)$. F_0 = Average fluorescence of 10 frames prior to electrical stimulation. F_{sat} = Maximal fluorescence upon electrical stimulation by 2 s stimuli train at 50 Hz.

Morphological Measurements

For morphological analysis, neurons were filled with 10 μM Alexa Fluor 594 (Life Technologies) in the patch pipet to obtain images of pyramidal neurons using a confocal microscope (Zeiss LSM 510). *Z* stacks of images were taken using a 63x objective, and two-dimensional maximal projection images were reconstructed using ZEN 2009 software (Zeiss). Spine analysis was performed on secondary and tertiary dendrites to reduce variability. Spines were manually outlined, and parameters (length, head width, and density) were measured in MetaMorph software (Molecular Devices). Each neuron was analyzed across multiple dendritic branches, pooling data for 50-100 spines in order to calculate mean values.

Immunofluorescence

Neurons were fixed with 4% paraformaldehyde/4% sucrose for 10 min at room temperature, permeabilized with 0.1% Triton X-100 in PBS for 5 mins at 4°C, blocked with 3% horse serum/0.1% crystalline grade BSA in PBS for 30 min at room temperature, and incubated with the indicated primary and secondary antibodies in blocking solution for 1 h at room temperature. The following antibodies were used in immunocytochemisty experiments: MAP2 (1:1000, mouse monoclonal, Sigma), vGlut1 (1:1,000, guinea pig polyclonal antibody AB5905, Chemicon), CaV2.1 (1:500, rabbit polyclonal 152-103, Synaptic Systems); CaV2.2 (1:100, rabbit polyclonal ACC-002, Alomone), GluA1 (1:4, rabbit polyclonal, Calbiochem), GluA2 (1:30 mouse monoclonal, Millipore), CB1R (L15; 1:1000; provided as a generous gift from Ken Mackie, Indiana University). The following secondary polyclonal antibodies (Invitrogen) were used: anti-rabbit AlexaFluor488 (1:500), anti-rabbit AlexaFluor546 (1:500), anti-mouse AlexaFluor546 (1:500), anti-mouse

AlexaFluor633 (1:500), and anti-guinea pig AlexaFluor546 (1:500). Neuron dendritic morphology was visualized by either MAP2 immunocytochemistry, or by sparse transfection of a GFP-expressing construct (L316). Neurons were randomly chosen, and images acquired using a TCS2 Leica confocal microscope with constant image settings. Z-stacked images were converted to maximal projection images and analyzed using MetaMorph Software with synaptic puncta quantified for puncta density per 10 μm of dendrite, size, and intensity.

GluA1 and GluA2 Surface Labeling

GluA1 and GluA2 surface labeling was performed essentially as described (Aoto et al., 2013). Briefly, culture neurons were washed with PBS containing 0.5 mM CaCl2 and 1mM MgCl2 (PBS^{MC}) with 4% sucrose. Neurons were preincubated at 37 C for 5 min with primary antibodies against GluA1 or GluA2 to allow labeling of surface AMPA receptors, washed with ice-cold PBS^{MC}, fixed with 4% PFA + 4% sucrose for 15min, then blocked in a detergent-free blocking soltion (PBS with 2% normal goat serum (Sigma), and 0.02% sodium azide) for 1 hr, followed by secondary antibody incubation at room temp for 1hr, mounted and imaged.

Fear Conditioning

Two-month-old male C57BL/6 mice (Charles River) were housed individually with normal 12/12 hr daylight cycle. They were handled daily for 5 days prior to training. On training day, mice were placed in fear-conditioning chamber (H10-11M-TC, Coulbourn Instruments) located in the center of a sound-attenuating cubicle (Coulbourn Instruments). The conditioning chamber was cleaned with 10% ethanol to provide a background odor. A ventilation fan provided a background noise at ~55 dB. After a 2 min exploration period, three tone-footshock pairings separated by 1 min intervals were delivered. The 85 dB 2 kHz tone lasted for 30s, and the footshocks were 0.75 mA and lasted for 2s. The footshocks coterminated with the tone. The mice remained in the training chamber for another 30s before being returned to home cages. In context test, mice were placed back into the original conditioning chamber for 5 min. The altered-context and tone tests were conducted in a new room. The same conditioning chamber was moved to this room and was modified by changing its metal grid floor to a plastic sheet, white metal side walls to plastic walls decorated with red stripes, and background odor of ethanol to vanilla. The ventilation fan was turned off to reduce background noise. Mice were placed in the altered chamber for 5 min to measure the freeze level in the altered context and after this 5 min period, a tone (85 dB, 2 kHz) was delivered for 1 min to measure the freeze to tone. The behavior of the mice was recorded with the Freezeframe software and analyzed with Freezeview software (Coulbourn Instruments). Motionless bouts lasting more than 1s were considered as freeze. Animal experiments were conducted following protocols approved by Administrative Panel on Laboratory Animal Care at Stanford University.

Open Field Force Plate Analysis

Mice were analyzed by the same standard force-plate actometer procedure as described previously (Fowler et al., 2003; Fowler et al., 2001). Analyses were performed before memory tests had been performed, and initiated by placing mice individually into the center of a force-plate actometer (28 cm x 28 cm). The actometer accurately monitors all mouse movements, allowing a precise quantitation of various types of movements over the observation period (15 min total, divided into three 5-min segments). The spatial confinement score reflects the deviation of the set of position coordinates in a session from the uniform distribution of the 64 separate 3.5×3.5 (cm) squares covering the entire force plate surface. The maximum score 99.216 indicated that a mouse (the center of force) stayed in one square for the entire session while the minimum score 0 indicated that a mouse equally visited each square. The distance was the total distance traveled in the session, which was the line integral of movement of the center of force. Low mobility bouts were defined as bouts during which the center of force remained inside a circle of 15-mm radius for more than 10 sec. The stereotypy score based on low-mobility bouts (LMB) was calculated as the movement of the center of force during low mobility bouts, expressed as distance per low mobility bout. Area measure was calculated as sum of triangle areas formed by three successive locations of the center of force in the session. The radius was another indicator of the spatial confinement, calculated as radius of the area of the points in this session. The stereotypy score (radius) was calculated as the distance divided by the radius measure per session. 25% center time was defined as the time in which the center of force (i.e., the mouse) remained inside the central square that occupies 25% of the actometer area.

Biochemical Measurements

For protein expression analysis of synaptic proteins as a consequence of loss of β-neurexin proteins in forebrain excitatory neurons, triple β-neurexin cKO animals were crossed with transgenic animals expressing Cre-recombinase under control of the CamKIIα promoter (The Jackson Laboratory, Strain Name: B6.Cg-Tg(CamK2a-cre)T29-1Stl/J). Protein levels were quantified in cortex homogenates from four pairs of adult littermate male mice using quantitative immunoblotting as described (Ho et al., 2006). Signals were detected with iodinated secondary antibodies, and monitored with a phosphoimager. Levels were normalized for the signals of control proteins (GDI and β-actin) blotted on the same blots to correct for differences in blotting efficiency. Antibodies used in this study for immunoblotting: Neuroligin-1 (1:1,000, mouse monoclonal antibody 4C12); Neuroligin-2 (170C2); Neuroligin-3 (1:1,500, rabbit polyclonal antibody 639B); PSD-95 (1:2,500, rabbit polyclonal antibody L667); GABAAα-Receptor (1:200, rabbit polyclonal antibody 06-868, Upstate); syntaxin-1A (1:1,000, rabbit polyclonal antibody 435B); Tomosyn (1:1,000, rabbit polyclonal antibody U5403); Liprin (1:2,000, rabbit polyclonal antibody 4396); CamKIIα (1:500, mouse monoclonal antibody C-265, SIGMA); SynGAP

(1:1,000, rabbit polyclonal antibody 4189); Shank3 (1:1,000, rabbit polyclonal antibody 1:1,000, Q9JLU4); Rab3A (1:1,000, mouse monoclonal antibody Cl42.2: Synaptic System); Rabphilin (1:1,000, rabbit polyclonal antibody I731); NSF (1:500, rabbit polyclonal antibody P944); Synaptophysin (1:2,000, mouse monoclonal antibody MAB5258, CHEMICON); Synapsins (1:2,500, rabbit polyclonal antibody P586); SCAMP (1:1,000, rabbit polyclonal antibody P936); SNAP-25 (1:2,500, mouse monoclonal antibody SM1-81, Sternberger Monoclonals); Synaptobrevin 2 (1:10,000, mouse monoclonal antibody 69.1, Synaptic System); synaptotagmin-1 (1:5,000, mouse monoclonal antibody Cl41.1, Synaptic System); Complexin 1/2 (1:1,000, rabbit polyclonal antibody P942); Munc-18 (1:500, mouse monoclonal antibody Clone 31, BD Transduction Labs); α-synuclein (1:1,000, rabbit polyclonal antibody T2270); β-actin (1:2,500, mouse monoclonal antibody AC-15, SIGMA); GDI (1:2,500, mouse monoclonal antibody 81.2, Synaptic System). For analysis of synaptic proteins as a consequence of loss of β-neurexin proteins in cultured cortical neurons, the following antibodies were used: Neurexins-CT (rabbit polyclonal antibody, A473); GluA1 (1:2000, mouse monoclonal antibody MAB2263); CaV2.1 (1:1000, rabbit polyclonal 152-103, Synaptic Systems); CaV2.2 (1:100, rabbit polyclonal ACC-002, Alomone), CB1R (CT; 1:1000; provided as a generous gift from Ken Mackie, Indiana University), NMDAR1 (1:1000, rabbit monoclonal antibody AB109182, AbCam).

GFP Immunoprecipitations and Immunoblotting

Cellular lysates were prepared by homogenizing brain tissue by sonication and 2 hours of extraction in immunoprecipitation buffer composed of phosphate-buffered saline (PBS) (pH 7.4; Sigma) supplemented with an additional 5mM HEPES-NaOH pH 7.4, 1% Triton X-100, 2mM CaCl2, and 2mM $MgCl_2$ and Complete protease inhibitors (Roche), followed by 1 h centrifugation at 100,000*g*. The resulting supernatant extract was used for protein concentration determination by BCA assay (Pierce). This Triton X-100 extraction was then normalized for protein concentration, and used for both direct immunoblot and immunoprecipitation experiments. Immunoprecipitation of GFP tag was performed using 5 μg of goat anti-GFP antibody (Rockland) and 10 μl of protein A-Sepharose beads (Amersham Pharmacia Biotech) added to the extracts. The mixtures were incubated for 1 h and washed three times with immunoprecipitation buffer, and proteins bound to the beads were eluted with sodium dodecyl sulfate (SDS) sample buffer. Samples were resolved on SDS-polyacrylamide gel electrophoresis (PAGE), transferred onto nitrocellulose membrane, and subjected to Western blot analysis using horseradish peroxidase (HRP)-conjugated secondary antibodies and the ECL Lumi-Light Western Blotting Substrate (Roche) detection system. Antibodies used for detection include GFP (rabbit polyclonal antibody, A11122, Invitrogen), and Neurexin-CT (rabbit polyclonal antibody, A473).

Neurexin-1β Bait Protein Pull-Downs

For recombinant Ig protein experiments, Ig-fusion constructs with and without neurexin1β (-SS4) were previously described (Boucard et al., 2005). To produce Ig-fusion proteins, HEK cells were cultured in 10-cm dishes until they reached 80% confluence. The medium was changed to fresh DMEM containing 25 mM chloroquine, and cells were incubated for 3 h and then transfected using calcium phosphate with 20 µg of cDNA. Media containing the soluble Ig proteins were harvested 4 days post-transfection and cleared by centrifugation at 1,000 × *g*. The supernatant was then adjusted to 10 mM HEPES-NaOH pH 7.4, 1 mM EDTA, and protease inhibitors (Roche Applied Science) and incubated overnight with protein A-Sepharose (GE Healthcare) to bind the human IgG Fc domain. The beads were then washed to remove unbound proteins, and whole brain cellular lysates were applied. Cellular lysates were prepared by homogenizing brain tissue by sonication and 2 hours of extraction in solubilization buffer composed of phosphate-buffered saline (PBS) (pH 7.4; Sigma) supplemented with an additional 5 mM HEPES-NaOH pH 7.4, 1% Triton X-100, 2mM $CaCl_2$, and 2mM $MgCl_2$ and Complete protease inhibitors (Roche), followed by 1 hour centrifugation at 100,000*g*. The resulting supernatant extract was incubated 1 hour with the Ig-Protein A beads, washed 3 times with solubilization buffer. Co-precipitated proteins were eluted with SDS sample buffer, and analyzed by SDS-PAGE immunoblotting.

Neuroligin-1/Neurexin-1 Interaction Assays

The entire coding sequences of 4 mice NL1 variants, NL1A1A2B, NL1A1A2^{-}B, NL1A1A2B^{-}, NL1A1A2^{-}B^{-} were cloned into pcDNA3.1 (Invitrogen) between HindIII and XhoI to yield pNL1A1A2B, pNL1A1A2^{-}B, pNL1A1A2B^{-}, and pNL1A1A2^{-}B^{-}, respectively. Coding sequences of NL1A1A2^{-}B, NL1A1A2B^{-}, and NL1A1A2^{-}B^{-} were generated by PCR-based mutagenesis using pNL1A1A2B whose coding sequence was obtained by RT-PCR from mouse brain mRNA. Splicing sites of A1, A2, and B to yield variants of Neuroligin 1 were described previously (Bolliger et al. 2008). pCMV-N1α FLAG encodes full-length neurexin-1α fused to a FLAG epitope lacking or containing an insert in splice site 4 (NRXN1α^{-SS4} and NRXN1α^{+SS4}), respectively, and were described previously (Boucard et al., 2005). pCMV-N1β FLAG encodes full-length neurexin-1β fused to a FLAG epitope lacking or containing an insert in splice site 4 (NRXN1β^{-SS4} and NRXN1β^{+SS4}), respectively, and were described previously (Boucard et al., 2005). HEK cells were co-transfected with 16 different combinations of plasmids encoding 4 NRXN1 variants and 4 NL1 variants. The empty plasmid, pCMV5 was also used as the mock control for NRXNs. Two days after the transfection, the cells were lysed in lysis buffer containing 20 mM Tris-HCl, pH 7.5, 100 mM NaCl, 4 mM KCl, 2 mM MgCl2, 2 mM CaCl2, 1% Triton X-100, protease inhibitor cocktail (Roche) for 1 h on ice. The samples were then centrifuged for 20 min at 20,000 g to remove insoluble materials and incubated with anti-Flag agarose beads (Sigma) for 1 h at 4°C. The beads were then washed four times with the lysis buffer and eluted with SDS sample buffer. The samples then analyzed by SDS-PAGE and immunoblotting. The input lanes were loaded with 2% of total protein extract used for immunoprecipitation. For the immunoblotting, fluorescently labeled secondary antibodies (donkey anti-rabbit IRDye 680CW, 1:15,000; donkey anti-mouse IRDye 800, 1:15,000; LI-COR Bioscience) were used and signals were detected with an Odyssey Infrared Imager and Odyssey software (LI-COR Biosciences). Signals for NRXN1s and NL1s were detected by the antibodies as follows: monoclonal mouse anti-NL1 antibody (4C12; 1:1000), polyclonal rabbit anti-Flag antibody (Sigma; 1:1000).

Statistics

Data are shown as mean ± SEM. Statistically significant differences (Student's t test or Paired Student's t test; * = $p < 0.05$; ** = $p < 0.01$; *** = $p < 0.001$) are indicated by asterisks.

Supplemental References

Anderson, G.R., Galfin, T., Xu, W., Aoto, J., Malenka, R.C., and Südhof, T.C. (2012). Candidate autism gene screen identifies critical role for cell-adhesion molecule CASPR2 in dendritic arborization and spine development. Proc Natl Acad Sci U S A *109*, 18120-18125.

Aoto, J., Martinelli, D.C., Malenka, R.C., Tabuchi, K., and Südhof, T.C. (2013). Presynaptic neurexin-3 alternative splicing trans-synaptically controls postsynaptic AMPA receptor trafficking. Cell *154*, 75-88.

Bolliger, M.F., Pei, J., Maxeiner, S., Boucard, A.A., Grishin, N.V., Südhof, T.C. (2008). Unusually rapid evolution of Neuroligin-4 in mice. Proc Natl Acad Sci U S A *105*, 6421-6426.

Boucard A. A., Chubykin A. A., Comoletti D., Taylor P., Südhof T. C. (2005) A splice code for trans-synaptic cell adhesion mediated by binding of neuroligin 1 to α- and β-neurexins. Neuron 48, 229–236

Burre, J., Sharma, M., Tsetsenis, T., Buchman, V., Etherton, M.R., and Südhof, T.C. (2010). Alpha-synuclein promotes SNARE-complex assembly in vivo and in vitro. Science *329*, 1663-1667.

Comoletti, D., Flynn, R.E., Boucard, A.A., Demeler, B., Schirf, V., Shi, J., Jennings, L.L., Newlin, H.R., Südhof, T.C., and Taylor, P. (2006) Gene Selection, Alternative Splicing, and Post-Translational Processing Regulate Neuroligin Selectivity for β-Neurexins. Biochemistry 45, 12816-12827.

Fowler, S.C., Birkestrand, B., Chen, R., Vorontsova, E., and Zarcone, T. (2003). Behavioral sensitization to amphetamine in rats: changes in the rhythm of head movements during focused stereotypies. Psychopharmacology (Berl) *170*, 167-177.

Fowler, S.C., Birkestrand, B.R., Chen, R., Moss, S.J., Vorontsova, E., Wang, G., and Zarcone, T.J. (2001). A force-plate actometer for quantitating rodent behaviors: illustrative data on locomotion, rotation, spatial patterning, stereotypies, and tremor. J Neurosci Methods *107*, 107-124.

Ho, A., Morishita, W., Atasoy, D., Liu, X., Tabuchi, K., Hammer, R.E., Malenka, R.C., and Südhof, T.C. (2006). Genetic analysis of Mint/X11 proteins: essential presynaptic functions of a neuronal adaptor protein family. J Neurosci *26*, 13089-13101.

Kaeser, P.S., Deng, L., Wang, Y., Dulubova, I., Liu, X., Rizo, J., and Südhof, T.C. (2011). RIM proteins tether Ca2+ channels to presynaptic active zones via a direct PDZ-domain interaction. Cell *144*, 282-295.

Maximov, A., Pang, Z.P., Tervo, D.G., and Südhof, T.C. (2007). Monitoring synaptic transmission in primary neuronal cultures using local extracellular stimulation. J Neurosci Methods *161*, 75-87.

Pang, Z.P., Cao, P., Xu, W., and Südhof, T.C. (2010). Calmodulin controls synaptic strength via presynaptic activation of calmodulin kinase II. J Neurosci *30*, 4132-4142.

Tabuchi, K., Blundell, J., Etherton, M.R., Hammer, R.E., Liu, X., Powell, C.M., and Südhof, T.C. (2007). A neuroligin-3 mutation implicated in autism increases inhibitory synaptic transmission in mice. Science *318*, 71-76.

Tabuchi, K., and Südhof, T.C. (2002). Structure and evolution of neurexin genes: insight into the mechanism of alternative splicing. Genomics *79*, 849-859.

Wozny, C., Maier, N., Schmitz, D., and Behr, J. (2008). Two different forms of long-term potentiation at CA1-subiculum synapses. J Physiol *586*, 2725-2734.

Xu, W., Morishita, W., Buckmaster, P.S., Pang, Z.P., Malenka, R.C., and Südhof, T.C. (2012). Distinct neuronal coding schemes in memory revealed by selective erasure of fast synchronous synaptic transmission. Neuron *73*, 990-1001.